Int J Earth Sci (Geol Rundsch) (2004) 93:860–885
DOI 10.1007/s00531-004-0423-6

ORIGINAL PAPER

A. Bandrés · L. Eguíluz · C. Pin · J. L. Paquette · B. Ordóñez · B. Le Fèvre · L. A. Ortega · J. I. Gil Ibarguchi

The northern Ossa-Morena Cadomian batholith (Iberian Massif): magmatic arc origin and early evolution

Received: 2 June 2003 / Accepted: 26 June 2004 / Published online: 20 August 2004

Abstract Diorites and related rocks in the Mérida area of northern Ossa-Morena (SW Iberia) are intrusive into Precambrian metavolcanic and metasedimentary sequences. Cumulate products from the H_2O-rich magmas are amphibole-rich gabbros to hornblendites. Major and trace element compositions, including Sr and Nd isotope data, allow the definition of a calc-alkaline series likely formed in relation to an immature arc setting. Crystallization of the intrusives has been established between ca. 570 and 580 Ma by U-Pb dating of constituent zircons. Garnet growth in dioritic rocks reflects a tectono–thermal overprint dated by Sm-Nd internal isochrons at around 555 Ma. Older Sm-Nd and Lu-Hf results between ca. 593 and 637 Ma on the same rocks suggest an earlier stage of regional metamorphism within the arc environment. The northern Ossa-Morena composite batholith and related metamorphic units have been tectonized and dismembered in the course of subsequent low-grade events during final stages of the Cadomian orogeny and the Variscan cycle. The units studied represent a well preserved segment of the arc region that evolved in Neoproterozoic times along the western border of Gondwana to conform the Cadomian–Avalonian basement of the Hercynian realm.

Keywords Cadomian · Geochronology · Garnet-bearing diorite · Geochemistry · Mérida

A. Bandrés · L. Eguíluz · B. Ordóñez
Dpto. de Geodinámica,
Universidad del País Vasco,
Aptdo. 211, 01006 Vitoria, Spain

C. Pin · J. L. Paquette · B. Le Fèvre
CNRS-UMR 6524 Magmas et Volcans,
Université Blaise Pascal,
63038 Clermont-Ferrand, France

L. A. Ortega · J. I. Gil Ibarguchi (✉)
Dpto. de Mineralogía y Petrología,
Universidad del País Vasco,
Aptdo. 644, 48080 Bilbao, Spain
e-mail: nppgiibi@lg.ehu.es
Tel.: +34-94-6012641

Introduction

Although often considered as a consequence of a simple orogenic evolution, recent comprehensive studies are increasingly showing that most orogenic belts are the result of polyorogenic histories that involved dispersal and amalgamation of lithospheric fragments, products of former orogenic activity (e.g., Nance et al. 1991; Nance and Thompson 1996; Von Raumer et al. 2003). The correct identification and characterization of the main continental growing episodes constitutes, therefore, a basic goal of the geological investigation. Within the Variscan foldbelt of central and western Europe, there occurs a number of realms, like the Bohemian, Armorican and Iberian Massifs, among others, where the pre-Variscan Neoproterozoic basement is well preserved showing striking similarities in the sedimentary, magmatic and tectono-metamorphic record (Murphy et al. 2002). It is nowadays agreed by most geologists working on those areas that these massifs and their American counterparts represent lithospheric blocks that originally formed a continuous Neoproterozoic peri-Gondwanan belt, the so-called Avalonian–Cadomian orogenic belt (D'Lemos et al. 1990; Murphy and Nance 1991; Murphy et al. 2002). Yet, Cambro–Ordovician, rift-related dispersion events, late-Paleozoic Variscan collision followed by pervasive transcurrent shearing and the opening of the Atlantic Ocean and ensuing dislocation overprint, obscured the Cadomian features within those areas. This greatly complicates a confident correlation among different massifs and the proper reconstruction of the former orogenic belt outline.

According to recent geodynamic reconstructions, the Avalonian–Cadomian belt recorded a protracted oblique subduction beneath the western border of Gondwana that caused island-arc formation at various places during Neoproterozoic times (750–570 Ma) and terminated diachronously with the development of a transform fault system from about 570 to 520 Ma. This was followed by the deposition of a Cambrian platformal sequence with Gondwanan fauna. During Cambrian–Ordovician times, the orogenic resultant structure was dismembered with the

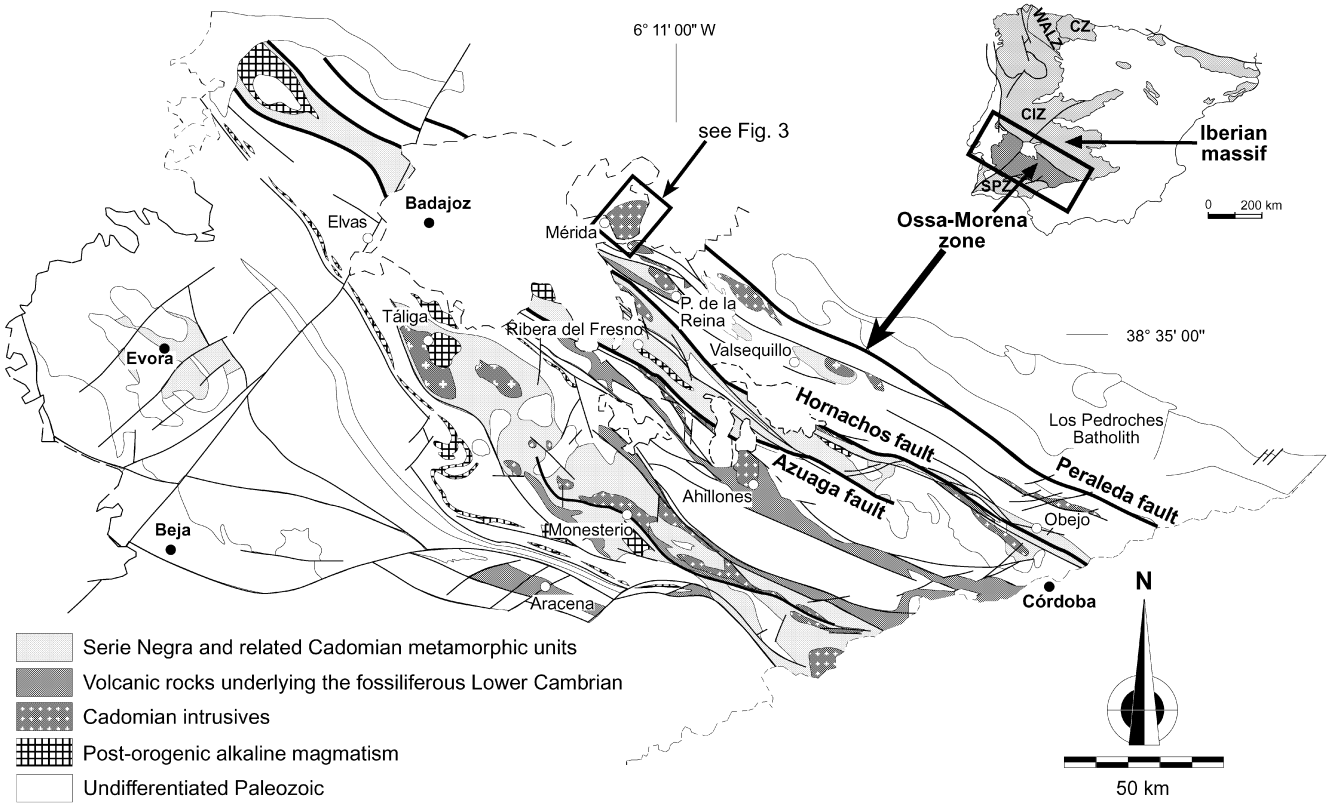

Fig. 1 Geological sketch map of the Ossa-Morena Zone showing the principal units related to the Cadomian orogeny (late Neoproterozoic to early Paleozoic rocks). *CA* Cantabrian zone, *WALZ* West Asturian-Leonese zone, *CIZ* Central-Iberian Zone

consequence of the Avalonian segment drifting westward to collide with Laurentia, while Cadomia remained relatively close to Gondwana (cf. Murphy et al. 2002 and references therein for a general review).

An accurate characterization of the different paleogeographical units within the pre-Variscan massifs of Europe appears therefore fundamental to a full understanding, interpretation and reconstruction of the original Avalonian–Cadomian belt. In this respect, the Iberian Massif provides the largest outcrop of Neoproterozoic rocks in Europe where limited deformation and metamorphism of some constituent regions during the upper Paleozoic Variscan orogeny reasonably preserved the pre-Variscan features, in particular within the so-called Ossa-Morena Zone (Fig. 1). There, the traces of Neoproterozoic to early Paleozoic (Cadomian) tectono-thermal events are recognizable in a number of areas. In this study, we present new petrological, geochemical and geochronological evidence for the development of arc-related units involving extensive calc-alkaline magmatic activity within northern sectors of the Ossa-Morena Zone. Associated tectono-metamorphic events are also documented and dated with respect to the main magmatic episode. These results should help to better constrain the Neoproterozoic geodynamic and paleogeographic evolution of this zone and its relative position with respect to the continental masses and Paleotethys Ocean. The chronological framework for the main episodes of the Cadomian history within the Iberian Massif is likewise improved.

Geological setting

The Ossa-Morena Zone (Fig. 1) comprises: (1) a southern domain (Monesterio), composed mainly of variably metamorphosed Neoproterozoic greywackes and shales, including a number of anatectic gneiss domes in the lowermost levels; (2) an elongated belt (Badajoz-Córdoba), comprising a rift-related bimodal volcanic suite of early to late Cambrian age that closed during late Cambrian times, and (3) a northern domain (Obejo-Valsequillo-Puebla de la Reina, OVPR), dealt with in the present study, composed mainly of plutonic and volcanic rocks weakly deformed during pre-Variscan and Variscan times. Strong deformation and associated polyphasic metamorphism reaching generalized anatexis affected mainly the southern domain during final stages of the Cadomian cycle. A lower Paleozoic continental shelf succession mainly Cambrian in age, for which a nondepositional gap of more than 30 Ma has been established, unconformably overlies the Cadomian basement.

The main geotectonic units in the Ossa-Morena Zone are separated by major strike-slip faults (Fig. 1). These faults have been interpreted as reworked Cadomian tectonic structures that controlled the Paleozoic sedimenta-

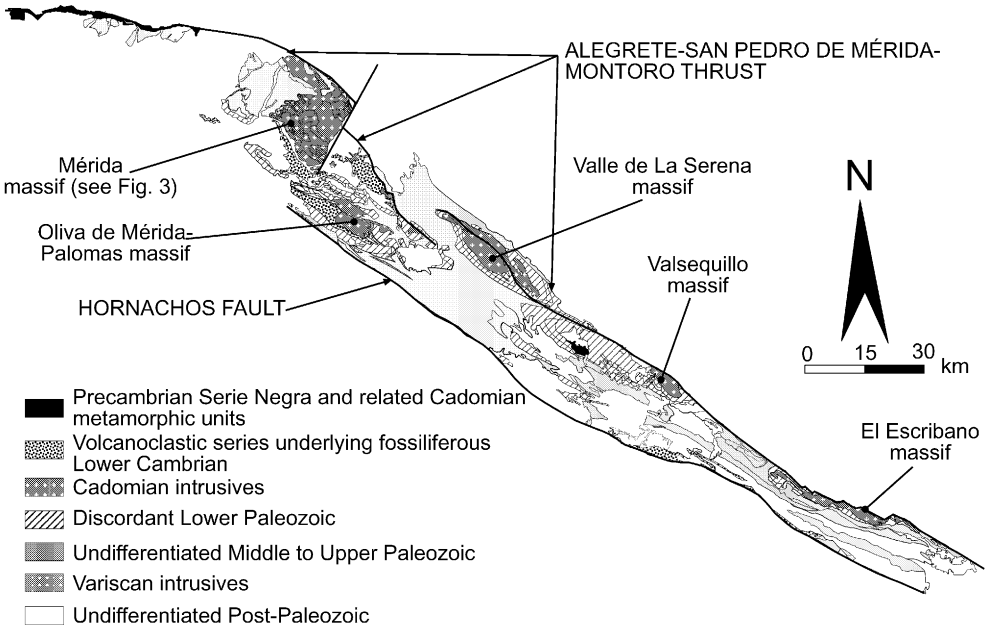

Fig. 2 Simplified geological map of the Obejo-Valsequillo-Puebla de la Reina domain of the northern Ossa-Morena Zone showing the main Cadomian Massifs

tion (during the subsequent orogenic cycle). One of the most important among these faults is the San Pedro de Mérida-Montoro Shear Zone (Peraleda fault of Castro 1988) that forms one of the boundaries of the study area (Fig. 1). This fault separates the Ossa-Morena Zone to the south from the Central-Iberian Zone to the north. The southern part of the Central-Iberian Zone adjacent to the shear zone corresponds to the Alcudian domain (Luso-Alcudian Zone of Lotze 1945). This is a weakly deformed area filled mainly by a thick clastic succession of turbidite-type sediments of upper Vendian age, including conglomerates with pebbles of phthanite similar to those found in the Ossa-Morena Zone (Vidal et al. 1994a, 1994b, 1999; Santamaría 1995; Pieren 2000). To the south of the San Pedro de Mérida-Montoro Shear Zone occurs the Obejo-Valsequillo-Puebla de la Reina study area which forms the northernmost domain of the Ossa-Morena Zone. The domain is bounded to the south by the Hornachos Fault (Fig. 1). Between the Hornachos Fault and the Azuaga Fault (Fig. 1) extends the Badajoz-Córdoba belt, a region that was strongly reworked by left-lateral faulting during Variscan times undergoing deformation and metamorphism that pervasively overprinted the Cadomian features.

The Obejo-Valsequillo-Puebla de la Reina (OVPR) domain crops out in the core of a number of sigmoidal structures defined by transcurrent faults (Fig. 1). This domain includes a pre-Ordovician sequence of Ossa-Morena affinity overlain by discordant Paleozoic series comparable to those of the Central-Iberian Zone, for which reason it has been classically considered as a transitional domain between the Ossa-Morena and Central-Iberian Zones (Julivert et al. 1972; Apalategui et al. 1983).

In detail, underlying Precambrian materials of the OVPR domain include two major lithological units (cf. Bandrés et al. 2002 for additional details on the lithostratigraphy of this domain) including (1) a low- to high-grade metamorphic unit, and (2) the Mérida-Montoro Igneous Complex. The lower member of the metamorphic unit may be correlated with upper portions of the Serie Negra (meaning 'black') formation from southern sectors of the Ossa-Morena Zone; i.e., with the Tentudía Group and, in part, the Montemolín Group (Eguíluz 1988; Eguíluz et al. 2000). Consequently, it will be here referred to as the Serie Negra of the OVPR domain. It is composed of metapelites containing abundant volcanic and volcanoclastic elements with minor intercalations of amphibolites and black quartzites. The overlying sections do not have exact lithological equivalents in southern Ossa-Morena. They consist of medium-pressure greenschists to amphibolites and a sequence of acid to intermediate volcanoclastic rocks, including massive rhyolite to dacite, known as the Don Álvaro sequence. This sequence grades laterally into a series of garnet-bearing micaschists, rhyolitic gneisses, glassy tuffs, low-grade tuffs and cinerites, with abundant occurrences of massive rhyolite, identified as a whole as the Oliva de Mérida volcanic series. Upwards, this volcanic series gradually passes into the pelitic sequence of the Alange Dam.

The Mérida-Montoro ultrabasic to acid igneous complex which constitutes the subject of our study, includes a number of intrusives outcropping more than 200 km near the localities of Mérida, Palomas, Oliva de Mérida, Valsequillo, Valle de La Serena and El Escribano (Fig. 2). Ultramafic, gabbro-diorite, tonalite and subordinate granite bodies are intrusive into all the above described metamorphic units. Among the associated volcanic to volcanoclastic rocks, the acid types predominate over the rocks of intermediate to basic composition. Variably deformed dioritic to granitic massifs elsewhere in the Ossa-Morena Zone (e.g., El Entredicho in the Badajoz-Córdoba

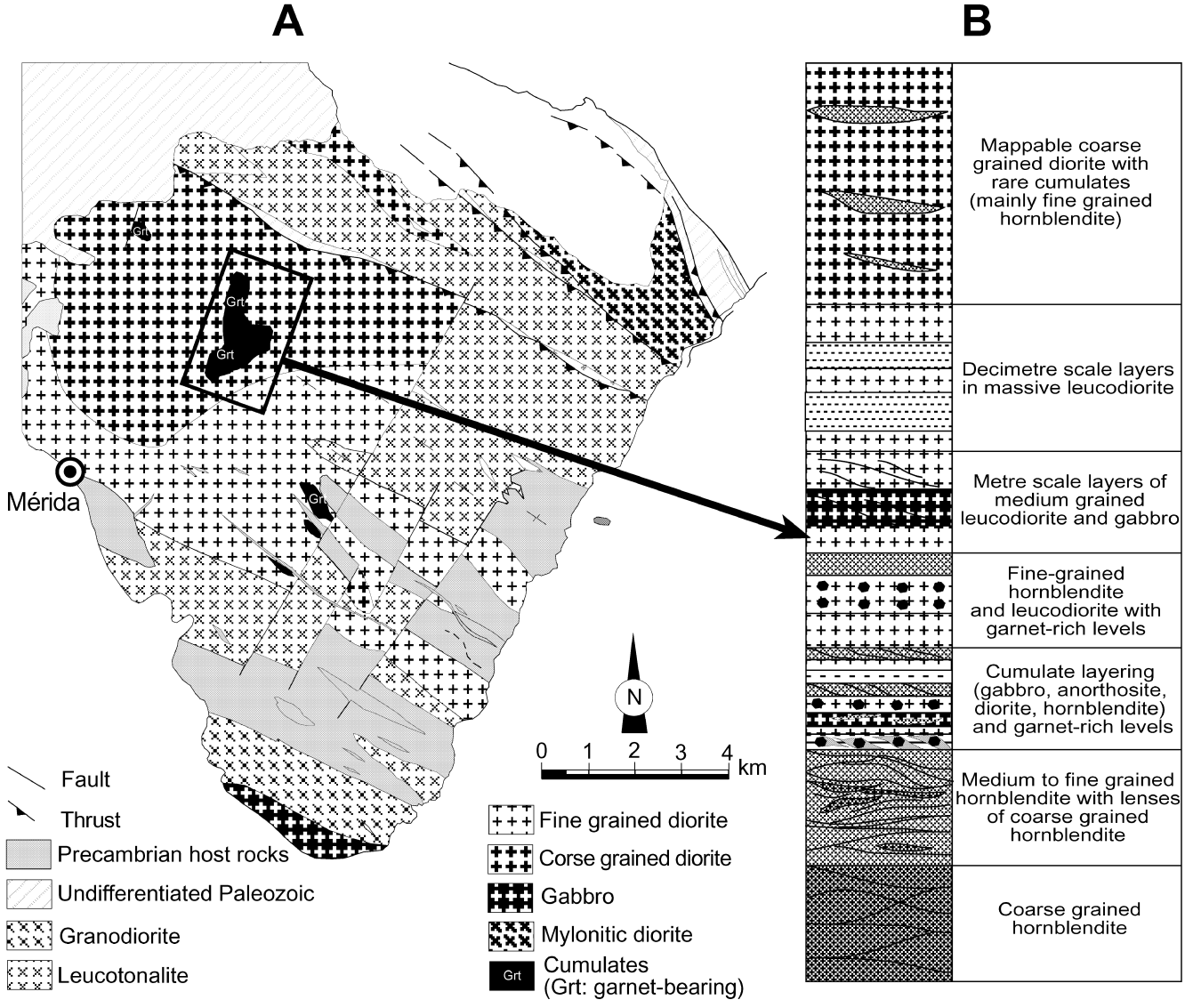

Fig. 3 **A** Geological sketch map of the Mérida Massif (cf. Figs. 1 and 2 for regional situation). **B** Schematic column showing the relationships between cumulates and related rocks from the Albarregas River section of the Mérida Massif

belt, Ahillones and El Mosquil to the south of this belt, etc.) exhibit petrographic features and field relationships that suggest a close genetic link with those of the OVPR domain.

Both intrusives and metavolcanics of the Mérida-Montoro Igneous Complex and the OVPR Serie Negra are discordantly overlain by either (1) nonmetamorphic volcanosedimentary rocks (equivalent to the early Cambrian Malcocinado formation from southern Ossa-Morena) that pass to an arkosic series of late Cambrian to early Ordovician age (intercalar series), or (2) more rarely, by the fossiliferous Archaeocyatha-bearing early Cambrian lime-stones (e.g., Alange; Fig. 2).

Structural features

Most rocks of the OVPR domain occurring below the pre-lower Paleozoic discordance, correspond to the plutonic rocks of the Mérida-Montoro Igneous Complex. Igneous and metaigneous rocks of this complex may be considered as belonging to a single batholith, tectonized and dismembered during the Variscan orogenic cycle. The resulting outcrops or massifs have been classically known as dioritoids of Palomas or Ahillones type (Apalategui et al. 1988). However, with the exception of some acid subvolcanic types which occur locally near Valsequillo and Palomas, most lithotypes described below are evenly found in the different massifs recognized. Among those massifs, the one at Mérida, where mappable plutonic units are best represented (Fig. 3), spans the most complete field and petrologic relationships. For this reason, it has

been studied in detail and will be taken as a reference for the petrographic and structural descriptions.

Mafic to felsic intrusives, related volcanic to volcanoclastic rocks and metasediments, and detrital overlying units were all affected by a system of shear bands. Deformation increases towards the E and SE and towards the N of the domain, which is towards the contacts with the Badajoz-Córdoba blastomylonitic belt and with the Central-Iberian Zone, respectively. Km-long and m-to-dam-thick shear bands exhibit gently sinusoidal morphology, spreading out or joining at the zones of maximum bending. Localized deformation along the bands becomes pervasive when these bands join, giving a gneissic appearance to the rocks. The shear zones affect the main lithological contacts and have a transpressive character of left-lateral movement with a NE-vergence thrust component. The vergence changes towards the SW in southern Ossa-Morena, defining a flower structure (Pereira 1999).

The original igneous features of the plutonic rocks are variably overprinted, or even erased, by the tectonic imprint that produced proto- to cataclasites and mylonites. Microstructures range from isotropic to planolinear mylonitic with abundant S-C structures. Pristine gabbros and cumulate rocks are preserved in the least deformed areas displaying cm-size cataclastic bands superposed onto the magmatic foliation. Less often, cm to dm ultramylonitic bands trending NNW-SSE and dipping 60° to 70° to the SW warp around or arrange parallel to the foliation. Lineations generally dip 40° to 60° to the NW. Zones of extensive deformation are particularly common in the rocks of dioritic composition which generally exhibit a discrete foliation, more pervasive towards the boundaries of the OVPR domain where it evolves into a protomylonitic to mylonitic foliation. Metre-sized (3–5 m) ultramylonitic zones parallel to the foliation are not uncommon. These zones trending NW-SE and dipping close to the vertical generally correspond to ancient acid dykes or slices of Paleozoic metasediments where deformation was focussed. Thus, within the shear zones, the acid intrusives are transformed into well-foliated orthogneisses with fine-grained protomylonitic matrix or, where stretching and grain size reduction were more intense, into mylonites, ultramylonites or phyllonites. These rocks show oriented feldspar phenocrysts in a fine-grained matrix with a strong stretching mineral lineation defined by quartz and biotite. The contacts of the intrusives with the host metasediments and metavolcanics are generally strongly tectonized. As a result, some dioritic massifs present zones of mylonites to ultramylonites up to 300 m thick trending ~N–S and dipping 60° to 80° to the W that mark the thrust contacts over highly deformed arkoses of Tremadoc age. Locally, late-stage faults and backthrusts associate a subvertical irregular foliation trending NNE that may transpose the previous regional foliation.

Metamorphic evolution and previous geochronology

The pre-Tremadocian metasediments and metavolcanic rocks of the OVPR domain were affected by a low- to high-grade regional tectono-thermal event. Evidence of contact metamorphism related to the emplacement of the diorites and related rocks of the Mérida-Montoro Igneous Complex is also preserved locally. Occasionally, the igneous rocks are transformed into orthogneisses and amphibolitic gneisses, although they usually show scarce evidence of deformation and metamorphism. A low- to very-low grade Variscan metamorphic overprint, which affected both the Cadomian basement and the Paleozoic cover sequences, is mainly developed along the main tectonic accidents that separate different areas in the OVPR domain. In those areas less affected by the Variscan overprint, it may be seen that the pre-Variscan synkinematic recrystallization reached medium- to high-grade amphibolite-facies conditions both in metabasites and metapelites (garnet–staurolite–biotite). In the course of the present study, rare hornblende–clinopyroxene–garnet metabasites have been found within the Serie Negra near Fuente Obejuna. These rocks provide maximum P–T conditions of 800 °C and >12 kbar, as estimated using published formulations for garnet–amphibole–plagioclase and garnet–clinopyroxene–plagioclase equilibria (Kohn and Spear 1990; Eckert et al. 1991; Krogh Ravna 1998 2000; cf. Table 1 for representative mineral analyses).

The age of the main metamorphic event in the northern Ossa-Morena units was established by Blatrix and Burg (1981) at ca. 550±10 Ma by Ar/Ar dating of metamorphic micas from low-grade metasediments of the Serie Negra in central sectors of the OVPR domain. Subsequently, Dallmeyer and Quesada (1992) provided two ages of ca. 551±3 and 552±3 Ma for hornblende concentrates from foliated amphibolites interbedded within the Oliva de Mérida metavolcanics. The same authors obtained an age of 562±1 Ma for muscovites of staurolite–garnet micaschists intercalated within the same series, which was interpreted together with the hornblende data, as a minimum age for the low- to medium-grade Cadomian metamorphism. The age of the igneous intrusives is instead poorly constrained. An attempt to date the dioritic rocks from Palomas by Martínez Poyatos (1997) by whole rock Rb-Sr methods provided 532±180 and 576±86 Ma. On the other hand, Bellon et al. (1979) obtained K-Ar dates on deformed feldspar porphyroclasts of gneissic rocks near Cerro Muriano. Their results (595±30 Ma) were interpreted to reflect a Cadomian tectonic event, although it appears likely that the rocks studied might rather belong to the adjacent domain of the Badajoz-Córdoba belt.

Table 1 Representative chemical analyses of clinopyroxene, garnet, amphibole and plagioclase

	OVPR metabasite			Garnet-bearing diorite			
Sample	BF18	BF18	BF18	BF18	81W	81W	81W
mineral	Cpx	Grt	Am	Pl	Grt-c	Grt-r	Am
SiO_2	52	38.8	42	59.3	37.5	37.7	41.5
TiO_2	0.06	0.24	1.55	bd	0.08	0.10	1.49
Al_2O_3	0.76	20.94	13.51	25.68	20.89	21.02	13.6
Cr_2O_3	0.01	0.04	0.11	bd	0.02	0.09	0.07
FeOt	13	21.3	17.1	0.04	31	27.1	16.5
MgO	10.4	2.45	8.9	0.02	4.57	4.56	9.3
MnO	0.44	1.69	0.36	bd	1.40	0.90	0.07
CaO	23.7	15.5	11.8	7.2	5.06	8.42	11.6
Na_2O	0.31	0.15	1.54	7.65	bd	bd	1.68
K_2O	bd	0.03	0.96	0.18	0.02	0.01	0.61
Total	100.7	101.1	97.8	100.1	100.5	99.9	96.4
Si	1.97	3.00	6.29	2.65	2.95	2.96	6.27
Ti	<0.01	0.01	0.17	-	<0.01	0.01	0.17
Al	0.03	1.91	2.38	1.35	1.89	1.91	2.42
Cr	<0.01	<0.01	0.01	-	<0.01	0.01	0.01
Fe^{3+}	0.05	0.08	0.21	-	0.11	0.08	0.23
Fe^{2+}	0.36	1.30	1.93	<0.01	1.93	1.70	1.85
Mg	0.59	0.28	1.99	<0.01	0.54	0.53	2.10
Mn	0.01	0.11	0.05	-	0.09	0.06	0.01
Ca	0.96	1.28	1.89	0.34	0.43	0.71	1.88
Na	0.02	0.02	0.45	0.66	-	-	0.49
K	-	<0.01	0.18	0.01	<0.01	<0.01	0.12

BF18 Clinopyroxene-garnet-bearing amphibolite from the Serie Negra of Fuente Obejuna: *81W* Garnet-bearing diorite from the Mérida massif. Cations and Fe^{3+}/Fe^{2+} estimated by charge balance criteria (cf. Droop 1987; Dale et al. 2000) assuming: 4 cations and 6 O (pyroxene *Cpx*), 8 cations and 12 O (garnet *Grt*; core/rim *c/r*); 23 O (amphibole *Am*); *Pl* plagioclase; *bd* below detection limits

The plutonic rocks of the Obejo-Valsequillo-Puebla de la Reina (OVPR) domain

The plutonic rocks of the OVPR domain intruded the Precambrian Serie Negra and related metasediments and metavolcanites of the Don Álvaro and Alange Dam sequences. The range of acid to ultrabasic igneous rocks may be grouped into several mappable units which most often show internal tectonic contacts. These units are as follows: (1) a dioritic unit, including gabbros and diorites that gradually pass into granodiorites, hornblendites and mafic cumulates, (2) a leucotonalitic unit, including a variety of rocks ranging in composition from tonalite to granodiorite, and (3) a granitic unit composed of biotitic granites. Fine-grained diorite, aplite and microgranite dykes cut across the various types of plutonic intrusives, but only the dioritic dykes (several m thick and >1 km long) can be mapped.

The dioritic unit

The dioritic unit consists of rocks ranging in composition from granodiorite to cumulate hornblendite and plagioclase-rich differentiates. Yet, the most abundant types have dioritic, quartzdioritic and monzodioritic composition. They generally form elongated bodies trending N–S, often bounded by tectonic contacts. Mixing relationships between the different dioritic facies are not uncommon. The main lithotype may be described as a holocrystalline, phaneritic, fine- to medium-grained (1–2 mm) diorite with seriated, inequigranular, pan-idiomorphic texture, composed of plagioclase ($An_{30–50}$) with albitic overgrowths, clinopyroxene with rims of green and green-brown amphibole, and biotite. Ilmenite, apatite, quartz and K-feldspar may occur as accessories. The plagioclase may appear in phenocrysts (<4 mm), occasionally defining a magmatic foliation. Besides these diorites, the following lithotypes are noteworthy within this unit as they constitute often mappable subunits:

Medium-grained gabbros with nearly undeformed hypidiomorphic texture (Fig. 4C) made of brown to dark green amphibole (ferroan pargasite to edenite), Ca-rich plagioclase ($An_{40–70}$) and clinopyroxene. Pyroxene and amphibole often exhibit intercrossed textures of cumulate origin. Ilmenite and titanite are accessories. The gabbros are often transformed into low-grade assemblages made of actinolite, chlorite, albite and quartz.

Light coloured coarse-grained quartzdiorites to granodiorites, made of plagioclase ($An_{10–30}$) and minor amounts of quartz and K-feldspar. There is some interstitial amphibole and the low-grade assemblage includes biotite, chlorite, epidote, clinozoisite and opaques. These rocks often contain partially resorbed, rounded to elliptical enclaves of fine-grained diorite.

Coarse-grained diorites are made of green amphibole and plagioclase ($An_{30–50}$) with equigranular, hypidiomorphic to allotriomorphic textures. The amphibole forms aggregates of subhedral crystals with relics of clinopyroxene and inclusions of opaques, apatite and titanite; it is often altered to fibrous actinolite, epidote and chlorite towards the rims. The plagioclase is generally replaced by epidote, clinozoisite, calcite and muscovite. The coarse-grained diorites contain abundant cumulate

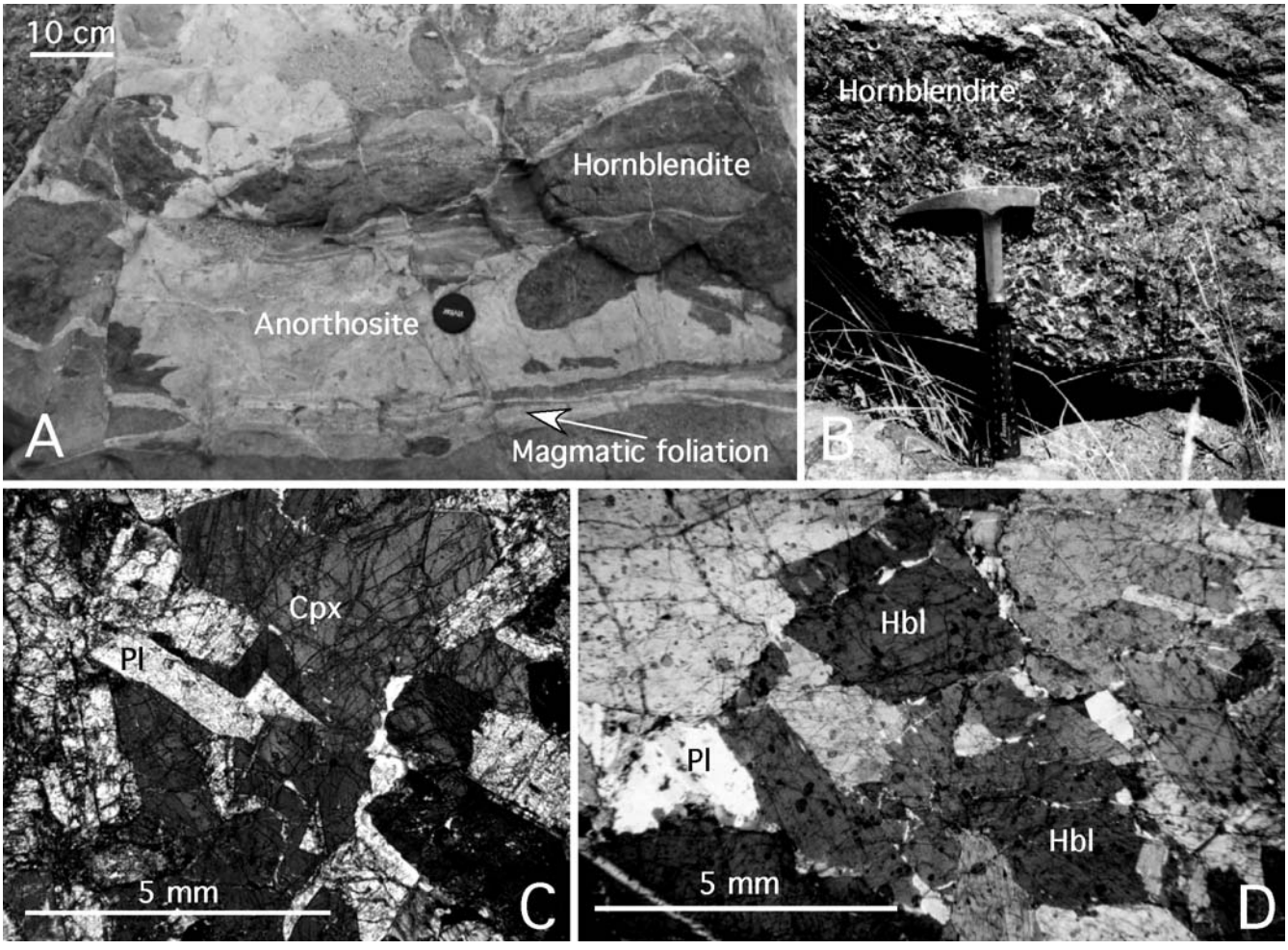

Fig. 4 **A** Field relationships showing magmatic contacts between plagioclase-rich differentiates and hornblendite of the Mérida Massif. **B** Coarse grained hornblendite from the Mérida Massif. **C** Gabbroic facies of the of the Palomas pluton showing subophitic texture defined by plagioclase (*Pl*) and clinopyroxene (*Cpx*). **D** Cumulate texture of hornblendite from the Albarregas River section showing rare plagioclase (*Pl*) crystals surrounded by subidiomorphic amphibole (*Am*)

horizons or layered facies (see below) and grade locally into medium- to fine-grained diorites. The fine-grained diorites are similar to the coarse-grained types, except that they may contain substantial amounts of interstitial quartz, likely related to the low-grade retrograde reactions. These rocks lack the layered textures but quite often bear evidence of magma mingling processes, albeit of magmas very similar in composition, containing enclaves of the more basic terms of the unit (coarse-grained diorites and cumulate gabbros). The fine-grained diorites are closely related to the granodioritic rocks and generally are not distinguishable as separate units in the maps.

Regarding cumulate rocks, hornblendites and other mafic cumulates form rare though conspicuous outcrops, up to more than 2 km long, notably within the Mérida Massif (Fig. 3). These rocks might correspond to the deepest portions of the igneous body as suggested by the local occurrence of garnet-bearing rock-types, which will be described separately. The cumulate rocks exhibit well-developed magmatic layering (Fig. 4A) locally bearing evidence of near solid state deformation during their emplacement. They evolve into gabbros or coarse-grained diorites. These are coarse (0.5 cm) to very coarse-grained (2–4 cm) magmatic adcumulates, rich in pargasitic amphibole with relics of clinopyroxene and plagioclase (Figs. 4A, B, D; 5A). Associated to the mafic cumulates occur small amounts of plagioclase-rich differentiates as lenses or irregular bodies (Fig. 4A, B) and, less often, as dam-size dykes that eventually intrude more evolved dioritic rocks.

The leucotonalitic unit

The rocks of the leucotonalitic unit are more homogeneous than those of the dioritic unit and range in composition from leucotonalite to granodiorite and monzogranite. Due to their deformation state they have often been described as orthogneisses (e.g., Gonzalo 1987). Yet, the intrusive contacts into the Neoproterozoic sequence are well preserved (e.g., Don Álvaro area), showing abundant xenoliths of host metasediments and induced thermal meta-

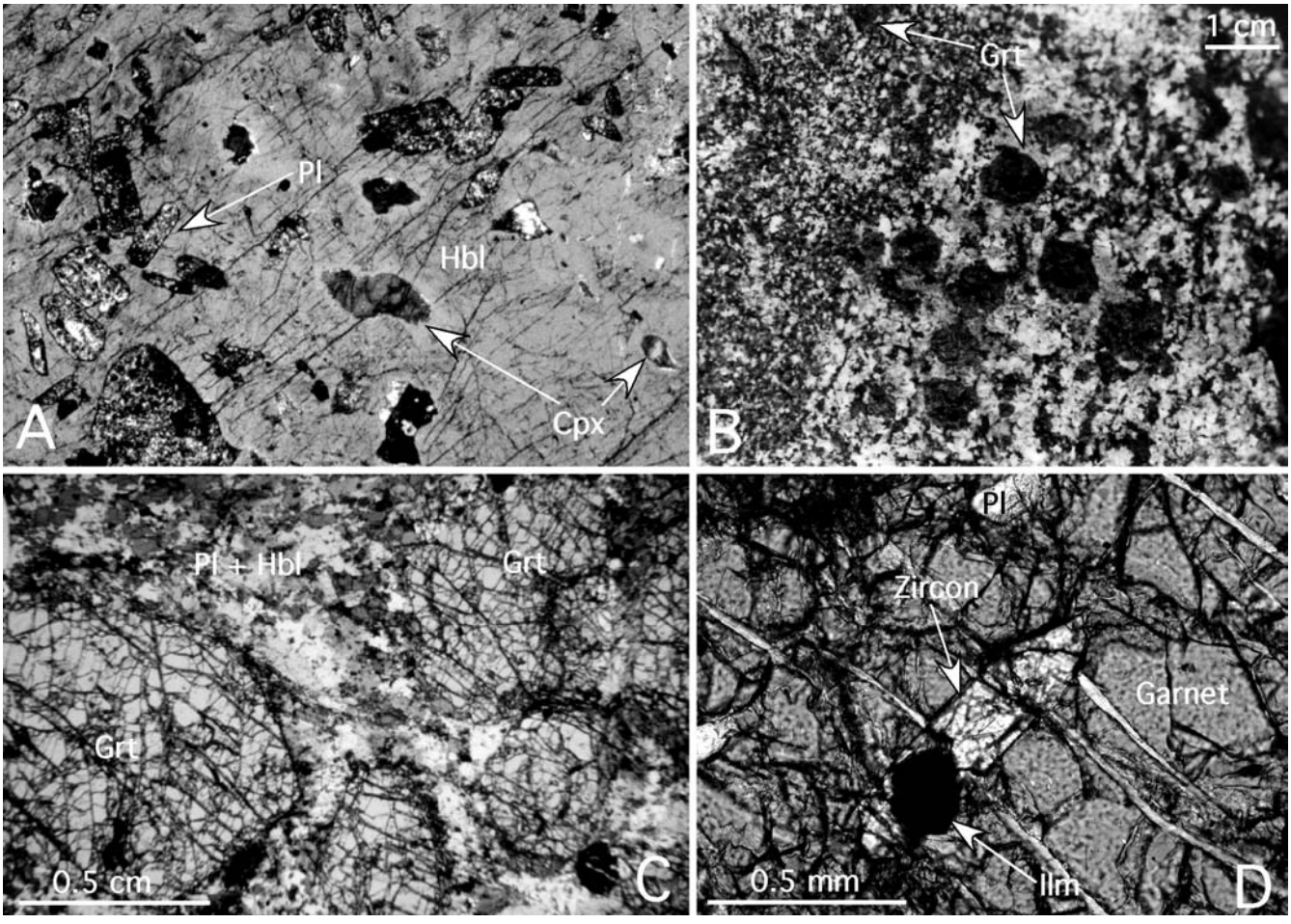

Fig 5 A Amphibole (*Am*) from coarse-grained hornblendite of the Mérida Massif showing relics of plagioclase (*Pl*) and clinopyroxene (*Cpx*) together with less abundant inclusions of ilmenite and rutile (not signalled). **B** Field view of the garnet-bearing diorites of the Mérida Massif; conspicuous large garnets are generally more abundant in the more leucocratic types like the one shown on the centre and right side of the picture. **C** Garnet-bearing diorite showing evidence of matrix grain size reduction (*Pl+Hbl*) and incipient foliation due to low-grade metamorphic imprint after garnet growth. **D** Inclusions of ilmenite (*Ilm*) and idiomorphic zircon representative of the zircons analysed by ID-TIMS within cm-sized garnet of the garnet-bearing diorites from the Mérida Massif

morphism. In general, these are fine- to medium-grained rocks made of plagioclase porphyroclasts, quartz, allotriomorphic perthitic K-feldspar and fine-grained biotite, with zircon, titanite, apatite and ilmenite as accessories. Low-grade retrogressive assemblages include quartz, epidote, biotite, chlorite and muscovite. These rocks show complex relationships with those of the dioritic unit. The field relationships suggest that the intrusion of the leucotonalites was coeval or slightly younger than the fine-grained diorites. In some sectors (e.g., Guareña), the rocks of the leucotonalitic unit cut the diorites resulting in processes of mixing and the local formation of medium-grained rocks of granodioritic composition.

The granitic unit

The granitic unit is mainly composed of cataclastic, holo-crystalline, phaneritic rocks with inequigranular, porphyritic, hypidiomorphic textures. They typically contain megacrysts (2–3 cm) of mesoperthitic orthose in a fine- to medium-grained seriated matrix of perthitic orthose, albite/oligoclase and globular quartz. Zircon, biotite, ilmenite and rare allanite occur as accessories. Epidote, clinozoisite, biotite, muscovite, chlorite and opaques are secondary phases. The granites are generally richer in biotite close to the contact with the rocks of the dioritic unit. Xenoliths of schistose metavolcanic and metasedimentary host rocks are found locally.

The garnet-bearing diorites and related rocks: petrography and P–T conditions

A remarkable feature of some diorites and, less frequently, of some of the associated cumulate ultramafic rocks of the dioritic unit (e.g., diorites of Mérida, Valdelapeña and Oliva de Mérida, Fig. 3A) is the oc-

currence of abundant cm-sized idiomorphic garnet, occasionally accompanied by a different type of finer-grained garnet ca. 2–4 mm in size (Fig. 5B, C, D). The garnets are generally more abundant in the more leucocratic types. The common paragenesis of these rocks is clinoamphibole (Mg-hornblende to ferroan pargasite) plagioclase ($An_{30–50}$), garnet ± clinopyroxene ± ilmenite/rutile defining a cumulate or intergranular igneous texture that would correspond to the transitional amphibolite-granulite facies conditions of the dioritic magma crystallization. The garnet-bearing rocks may bear evidence of deformation and matrix grain-size reduction (Fig. 5C), although they often preserve igneous textures that attest to a complex crystallization sequence whereby garnet-rich hornblendites evolved into coarse-grained, layered diorites to plagioclase-rich rocks with or without garnet. Additionally, well-foliated leucodiorites sometimes contain just fine grained idiomorphic garnet. In this case, the garnet occurs concentrated along localized zones parallel to the main foliation defining granonematoblastic textures that can be interpreted as having been formed during solid-state deformation. Sporadic plagioclase enrichments surrounding the idiomorphic garnets in these metadiorites suggest limited partial melting and a peritectic character of the garnet in these rocks.

The large idiomorphic garnets often present two texturally distinct regions. Inner areas account for most of the garnet diameter and are rich in inclusions of plagioclase ($An_{38–45}$) and, less often, ilmenite and zircon. They are poorly zoned, with typical compositions around $Alm_{65}Grs_9Prp_{19}Sps_4And_3$. Outer portions of these garnets represent less than 25% of the garnet diameter. They are limpid and often distinctly richer in Ca and poorer in Fe than the garnet inner region, with compositions around $Alm_{57}Grs_{17}Prp_{20}Sps_3And_3$. Where these two distinct regions are not clearly depicted, there appears to exist a consistent pattern of moderate X_{Fe} decrease and Ca increase from core to garnet rims. The smaller, idiomorphic and unzoned garnets within the same samples, and also those in the foliated leucodiorites, are inclusion-free and have compositions similar to the outer portions of the large garnets (Table 1). Finally, an inversion of the zoning patterns is observed near the rims of some garnets, with an increase in Fe and Mn contents and decrease in Ca and Mg interpreted to reflect limited intracrystalline diffusion during retrograde events.

The Ca and X_{Mg} increase towards the rims is generally attributed to garnet growth under progressively higher P and T conditions (Spear 1993 and references therein). However, the extent of this variation may vary greatly depending on the composition of other phases in equilibrium with garnet. In the present case, the change in composition is sometimes sharp and always related to a change in the texture of this mineral, whereby newly grown, Ca-rich garnet would form around large inclusion-rich garnets, but also as discrete small grains in the rock matrix. Assuming that garnet equilibrated initially with those minerals that may best preserve the composition of the magmatic stage (that is, Ca-rich plagioclases and Ti, Na and Al-rich brown/green hornblende), the P–T conditions estimated for this phase using garnet–amphibole–plagioclase equilibria (Kohn and Spear 1990; Krogh Ravna 2000) were ca. 750 °C, 5.5 kbar (cf. Table 1 for representative mineral analyses). These P–T estimates are somewhat lower than those assumed to prevail under transitional amphibolite–granulite facies conditions (e.g., Pattison 2003), which may be the result of partial re-equilibration of the garnet inner regions following crystallization of the dioritic magma. The P–T conditions calculated following the same procedure for a hypothetical stage of renewed garnet-growth, richer in grossular molecule and in equilibrium with ca. An_{30} plagioclase and common hornblende, are near 800°C and 11 kbar, that is, very similar to those recorded by the highest-grade metabasites of the OVPR metamorphic units (cf. section 'Metamorphic evolution'). It may be noted that pressures up to more than 15 kbar at slightly higher temperatures could also be deduced using the composition of abundant Ca-poor plagioclase (ca. An_{10} and less) in the same rocks. However, such P–T estimates call for some precaution since this albite might result of the low-grade metamorphic overprint that affected most of these rocks.

Geochemical and isotopic results

In order to constrain the igneous crystallization age of the northern Ossa-Morena batholith, zircons extracted from one diorite and one intrusive granite body have been analysed for U-Pb isotopes. Garnet whole-rock pairs from the garnet-bearing diorites have also been analysed for Sm-Nd and Lu-Hf radiogenic isotope systems in order to put constraints on the age of the garnet-forming, high-grade metamorphic events within the OVPR domain. Moreover, the geochemical characteristics of a set of 23 mafic to felsic rocks have been studied, mostly on the basis of selected immobile trace elements. Some of these samples have also been analysed for Sr and Nd isotopes, in order to further characterize the source reservoirs and the petrogenetic evolution of the igneous suite.

U-Pb zircon geochronology

Garnet-bearing diorite of Mérida

Abundant zircon crystals were extracted from a garnet-bearing diorite within the cumulate facies of the Mérida Massif (sample MER). Zircons in this rock occur primarily within the inclusion-rich, inner portions of cm-size garnets. The zircon grains, up to 1 mm long, are light-yellow, translucent and devoid of inclusions. The crystals are euhedral and short prismatic often with rounded geometric faces indicating crystallization in equilibrium with garnet (Fig. 5D). Five air-abraded fractions have been analysed by ID-TIMS methods (Table 2). The radiogenic Pb contents are 25–30 μg/g. The five analytical

Table 2 U-Pb data for zircons of the garnet-bearing diorite from the Mérida massif (sample MER). Absolute errors in percent are given at the 2σ level. Numbers in brackets represent the number of grains in fraction; *eu* euhedral

Fraction	Weight	Concentrations		Atomic ratios					Apparent ages (Ma)		
(μm)	(μg)	U	Pb_{rad}	$^{206}Pb^{a}$	$^{208}Pb^{a}$	$^{206}Pb^{b}$	$^{207}Pb^{b}$	$^{207}Pb^{b}$	206Pb	207Pb	207Pb
		(ppm)	(ppm)	204Pb	206Pb	238U	235U	206Pb	238U	235U	206Pb
Z1: [2] eu	27	280	25.5	2878	0.0745	0.09369 (0.31%)	0.7662 (0.49%)	0.05932 (0.36%)	577	578	579
Z2: [5] eu	77	213	19.9	1704	0.0856	0.09388 (0.23%)	0.7674 (0.29%)	0.05929 (0.17%)	578	578	578
Z3: [3] eu	52	205	18.6	4327	0.0734	0.09368 (0.20%)	0.7662 (0.34%)	0.05932 (0.26%)	577	578	579
Z4: [3] eu	38	339	30.9	4472	0.0739	0.09370 (0.24%)	0.7657 (0.33%)	0.05926 (0.22%)	577	577	577
Z5: [3] eu	37	273	25.0	3159	0.0784	0.09367 (0.22%)	0.7660 (0.35%)	0.05931 (0.26%)	577	577	578

[a] Measured ratio (cf. analytical techniques)
[b] Calculated ratio (cf. analytical techniques)

points are concordant, defining a pooled $^{206}Pb/^{238}Pb$ age of 577.5±0.6 Ma (Fig. 6).

Porphyritic granite of Valle de la Serena

The Valle de la Serena Massif consists of variably deformed porphyritic granites and diorites that intrude the acid rocks. A sample of deformed porphyritic granite (sample ZALA) was collected in the vicinity of the Higuera de la Serena village for U-Pb isotopic analysis of zircon by SHRIMP methods. The zircons extracted are mainly pink, from transparent to opaque and generally with euhedral and elongated shape and, in some cases, rounded faces. Cathodoluminiscence images reveal magmatic oscillatory domains with some zircons showing growth discontinuities (e.g., zircons 20, 25; Fig. 7) and, occasionally, well discriminated inner cores surrounded by oscillatory rims (e.g., zircon 6; Fig. 7). The dominant pattern is that of uniform planar oscillatory zoned zircons (e.g., zircon 29; Fig. 7). All the domains analysed have a typical magmatic Th/U ratio around 0.7–0.3 (Table 3). There is not a fractionation of Th and U with respect to the $^{208}Pb/^{206}Pb$ ratio, therefore we used the concordia diagram using the ^{208}Pb correction method. Spots 16.1 and 34.1 have a high common lead contribution and are offset from the main Gaussian-distributed cluster made up by 7 domains within 7 zircons. This cluster yields an average $^{206}Pb/^{238}U$ age of 573±14 Ma (WM; 573±16 Ma, NM; concordia diagram, Fig. 8).

Garnet whole-rock Sm-Nd and Lu-Hf geochronology

Garnet-bearing diorite of Mérida

Three samples of garnet-bearing diorite within the cumulate facies of the Mérida Massif have been investigated for Sm-Nd isotopes. The analytical results are presented in Table 4. Internal isochrons calculated from the Sm-Nd data for the garnet-bearing diorites yield the following results: (1) whole rock sample BM105 plus constituent, barely zoned, cm-size garnet = 557±3.7 Ma (Fig. 9A); the same garnet plus constituent amphibole yields 564.1± 3.7 Ma (Fig. 9A), while the three fractions (whole rock, garnet, amphibole) taken together result in exceedingly high error values of more than 50 Ma; (2) whole rock sample MER1 plus similar cm-size garnet = 563.9± 2.5 Ma (Fig. 9C); (3) the spatially associated sample MER2 provides a distinctly older, although less precise, internal (whole rock-centimetric garnet) age of ca. 592.7± 7.9 Ma (Fig. 9D).

In view of the relatively low Sm/Nd ratios of analysed garnets, suggestive of the presence of light rare earth (LREE)-bearing microinclusions, one fraction of the garnet from sample BM105 was leached following a procedure modified from Zhou and Hensen (1995) to minimize the effect of contamination from eventual LREE-rich inclusions. The Sm/Nd ratio thus obtained for

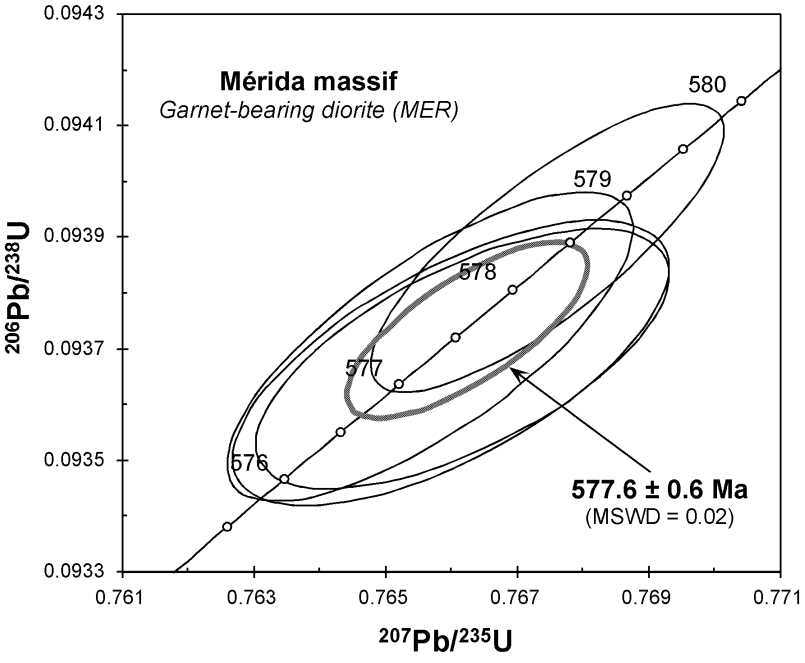

Fig. 6 U-Pb Concordia diagram for the Garnet-bearing diorite of the Mérida Massif (ellipse errors are 2σ, cf. analytical techniques)

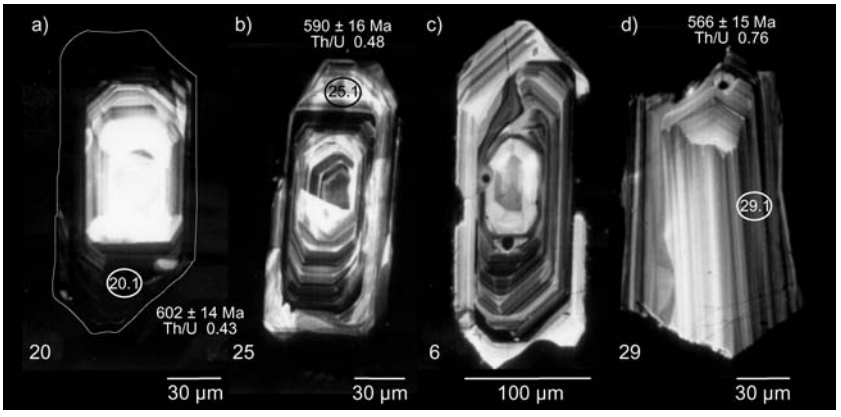

Fig. 7 Cathodoluminiscence images from zircon sections of the porphyritic granite (ZALA) of the Valle de La Serena Massif. **A** zircon 20; **B** zircon 25; **C** zircon 6; **D** zircon 29

Table 3 Ion-microprobe isotopic data of single zircons from the porphyritic granite of the Valle de La Serena massif (sample ZALA)

Spot	U	Th	Pb[c]	Th/U	f^{206}Pb	^{206}Pb/^{238} U[b]	^{207}Pb/^{235}U[b]	^{206}Pb/^{238} U apparent age	CL pattern
	ppm	ppm	ppm		(%) [a]			(Ma±1σ)	
Protholith									
13.1	227	105	21	0.46	0.38	0.0894±26	0.716±33	552±15	Rim oscillatory
20.1	488	210	49	0.43	0.00	0.0979±25	0.806±27	602±14	Rim oscillatory
24.1	384	137	36	0.36	0.08	0.0922±25	0.770±36	569±13	Oscillatory
25.1	202	96	20	0.48	0.41	0.0958±27	0.813±35	590±16	Rim oscillatory
29.1	160	121	16	0.76	0.00	0.0918±25	0.788±36	566±15	Oscillatory
30.1	207	100	20	0.48	0.56	0.0913±25	0.707±37	563±15	Oscillatory
33.1	145	48	13	0.33	0.51	0.0920±27	0.761±38	567±16	Oscillatory
Pb-less									
16.1[d]	858	291	75	0.34	0.48	0.0872±67	0.708±133	539±40	Rim oscillatory
34.1[d]	193	123	17	0.64	0.99	0.0839±109	0.643±147	520±65	Oscillatory

Ratios corrected for common lead (^{208}Pb correction method)
[a] Percentage of common ^{206}Pb relative to total measured ^{206}Pb
[b] Standard deviation (1σ) refers to the last significant digits of the corresponding ratios
[c] Radiogenic Pb
[d] Denotes outliers from the mean age

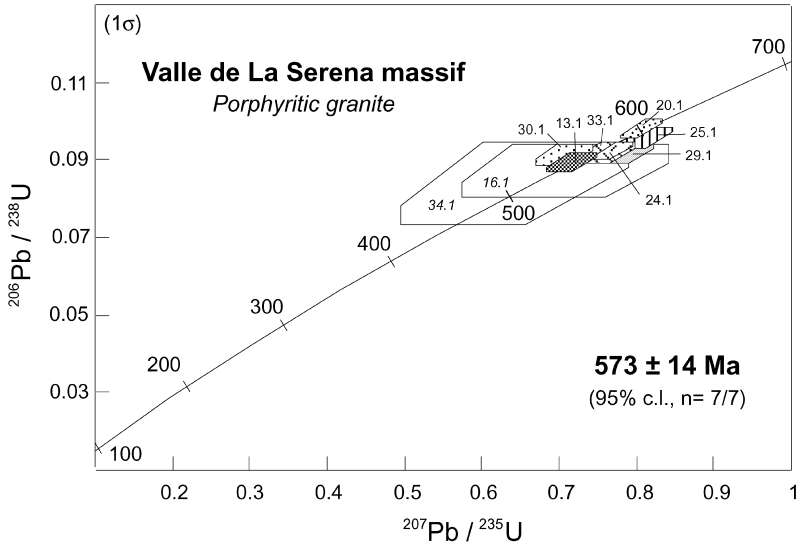

Fig. 8 U-Pb concordia diagram for zircons from a deformed porphyritic granite (ZALA) of the Valle de La Serena Massif. Numbers written in italics denote outliers from mean age. *n* denotes 7 spots on 7 zircon crystals. 573±14 Ma is the average $^{206}Pb/^{238}U$ age excluding spots 16.1 and 34.1 with a high common lead contribution

Table 4 Sm-Nd geochronological data for the garnet-bearing diorites of the Mérida Massif

Sample	Sm	Nd	$^{147}Sm/^{144}Nd$	$^{143}Nd/^{144}Nd$	Internal age
	(ppm)	(ppm)			(Ma)
BM105 wr	1.53	6.05	0.1520	0.512588±5	
BM105 Am	1.4	5.56	0.1538	0.512571±5	
BM105 Grt (unleached)	24.5	22.6	0.6584	0.514436±6	557±3.7 (Grt-wr) 564.1±3.7 (Grt-Am)
BM105 Grt (leached)	20.92	7.85	1.606	0.517861±4	553.4±1.7 (Grt-wr) 555.9±1.7 (Grt-wr)
MER1 wr	6.60	22.3	0.1789	0.512710±5	
MER1 Grt	2.77	1.65	1.018	0.515808±6	563.9±2.5 (Grt-wr)
MER2 wr	5.29	21.5	0.1485	0.512579±7	
MER2 Grt	2.66	4.28	0.3751	0.513459±5	592.7±7.9 (Grt-wr)

Grt garnet; *Am* amphibole; *wr* whole rock

the leached garnet fraction was increased by a factor of three providing a more precise and slightly younger whole rock-leached garnet age of 553.4±1.7 Ma (Fig. 9B), or amphibole-leached garnet age of 555.9±1.7 Ma (Fig. 9B); again, the error on the calculated age considering the whole rock, leached garnet and amphibole fractions together is extremely high, around ca. 28 Ma.

One sample (MER3) of the garnet-bearing diorites has been also analysed by multi-collection ICP-MS for Lu-Hf isotopes (Table 5). In order to avoid the effect of the zircon inclusions in this mineral, the garnet was selectively dissolved with HF. The age obtained for a whole rock-garnet pair: 637±40 Ma (95% confidence level; Fig. 9E), is rather imprecise due to the small difference in the measured Lu/Hf ratios of the garnet and whole rock, and overlaps the Sm-Nd ages within error. By including the data for whole rock sample MER1, the calculated age is 654±23 Ma (MSWD=0.8).

Whole rock major and trace element compositions

Major element composition of samples analysed is given in Table 6 and illustrated in Fig. 10 using silica variation diagrams. The silica contents range from 46.3 to 77.4%. MgO and CaO contents systematically decrease with increasing SiO_2, whereas Na_2O, K_2O and P_2O_5 contents increase. However, the analytical data show high dispersion in most diagrams (e.g., Al_2O_3, MgO, K_2O, Na_2O) precluding a linear distribution with respect to silica. The classification of the intrusive rocks studied into (1) cumulates, (2) diorites, and (3) leucotonalites is based on the petrographic and textural characteristics, yet this scheme is mainly in agreement with the geochemical data as shown in Fig. 11A. The mobility of K_2O may be, in part, responsible for the observed variation from low-K to shoshonitic compositions (Fig. 10). Yet, most samples plot in the fields of low- to medium-K magmatic rocks (Fig. 10) and, in spite of the observed dispersion, the whole set of samples defines a trend consistent with a calc-alkaline series (Fig. 11A, B). Moderate Mg numbers [Mg/(Mg+Fe)=0.6–0.4] and moderate to low levels of Cr, Ni and Co (<350, 150 and 70 ppm, respectively) point to slightly evolved magmas.

Incompatible trace element abundances show considerable diversity in connection with the variations in SiO_2 contents. Chondrite-normalized (Evensen et al. 1978) REE plots allow us to distinguish a number of patterns among the rocks of the Mérida Massif. Most of them indicate a systematic enrichment in light rare earth ele-

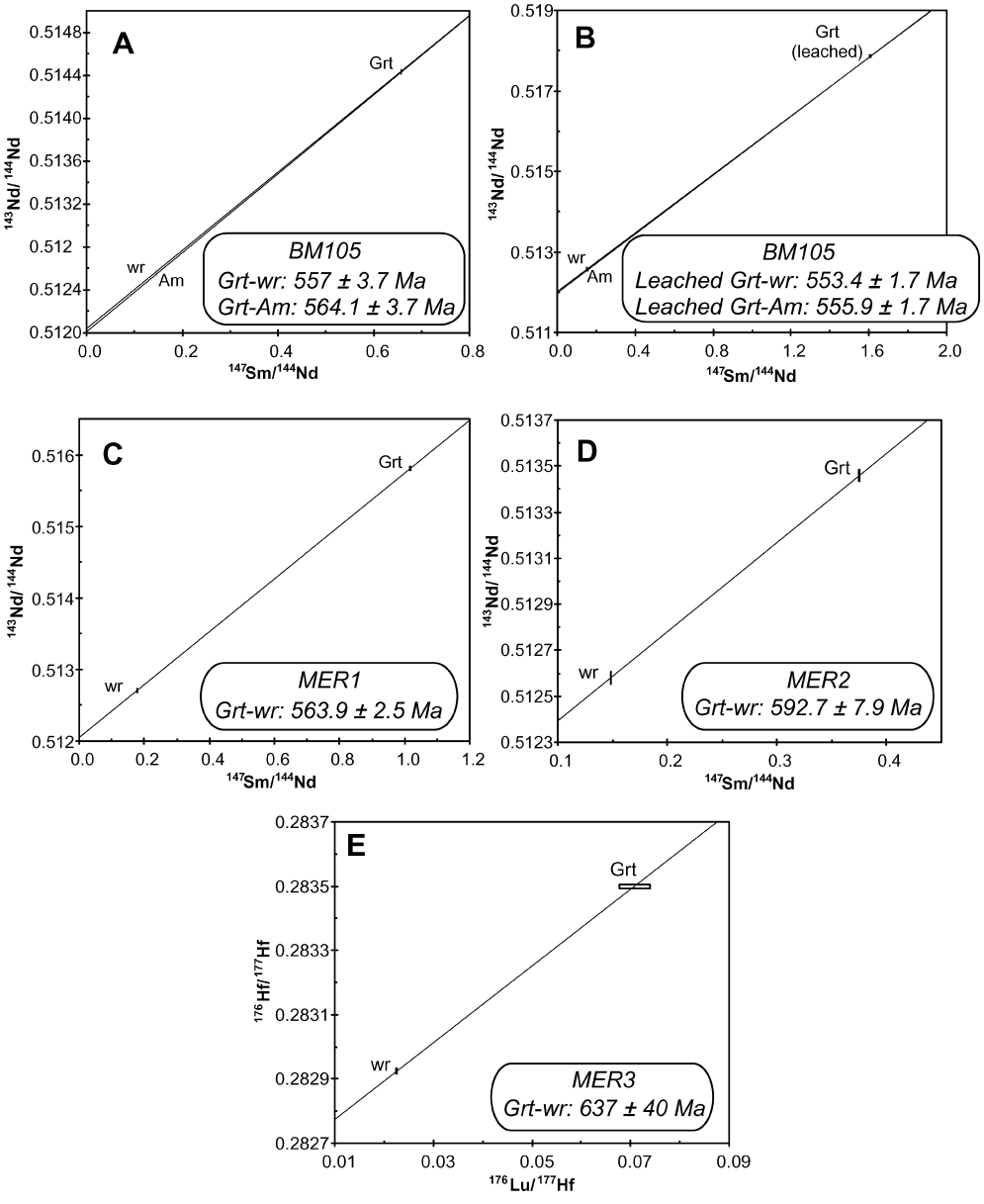

Fig. 9 Sm-Nd and Lu-Hf internal isochrons for minerals and whole rocks of garnet-bearing diorites from the Mérida Massif

Table 5 Lu-Hf geochronological data for the garnet-bearing diorites of the Mérida massif

Sample	Lu (ppm)	Hf (ppm)	$^{176}Lu/^{177}Hf$	$^{176}Hf/^{177}Hf$	Internal age (Ma)
MER1 wr	0.594	1.893	0.0447±4	0.283198±5	
MER2 wr	0.252	1.475	0.0243±1	0.283018±14	
MER3 wr	0.287	1.812	0.0226±1	0.282925±8	
MER3 Grt	3.03	6.10	0.0708±3	0.283500±4	637±41 (Grt-wr)

Grt garnet; *wr* whole rock

ments (LREE), except some diorites and leucotonalites from the San Pedro area. The first group (mainly composed of gabbros from Alange and granodiorites from the Don Álvaro areas) is characterized by low REE contents (ΣREE <57 ppm), LREE enrichment [$(La/Lu)_n$ =5.6±2.1] and large Eu positive anomalies (Eu/Eu*=1.5±0.43; group A). Some cumulative rocks are richer in REE (ΣREE= 89±11 ppm) and show LREE enriched patterns ($La/Sm)_n$=4.9±2 with large Eu negative anomalies (Eu/Eu*=0.55±0.05; group B). Yet, most cumulative rocks are REE-rich (ΣREE=110±40 ppm) with fractionated REE patterns [$(La/Lu)_n$=7.6±3.0; $(La/Sm)_n$=3.2±0.7] and weak negative or slightly positive Eu anomalies (Eu/Eu*= 0.92±0.12; group C). Three samples of this group slightly

Table 6 Whole rock major and trace element compositions of diorites and related rocks from the Mérida Massif

Sample	BM4	BM105	BM26	BM27	BM28	BM29	BM30	BM14	BM31	BM32	BM33	BM34	BM35	BM21	BM40	BM51	BM59	BM48	BM62	BM62B	BM15	BM18	BM20	BM23
Rock type	Cum	Cum	Cum	Cum	Cum	Cum	Pl-dif	Di-grd	Di-grd	Di-grd	Di-grd	Di-grd	Di-grd	Di-grd	Di-grd	Di-grd	Di-grd	Gabbro	Grd	Grd	Lc	Lc	Lc	Lc
SiO_2	47.6	46.3	55.6	61.6	49.9	46.6	72.1	49.4	53.4	58.8	56.4	53.4	55.5	57.9	49.2	46.9	58.4	51.0	59.3	65.4	73.8	77.4	71.7	73.9
TiO_2	1.11	1.09	1.55	0.93	0.76	1.2	0.14	0.99	0.56	0.69	0.81	0.72	0.66	0.71	0.58	0.75	0.56	0.96	0.5	0.36	0.05	0.02	0.14	0.11
Al_2O_3	15.0	21.5	12.9	15.9	16.6	15.7	14.5	18.5	17.0	17.0	16.8	14.9	14.8	16.1	22.5	19.2	17.0	17.0	19.6	16.4	14.2	13.4	14.5	14.8
Fe_2O_{3t}	11.6	11.1	10.7	6.1	7.9	11.8	1.8	9.9	7.4	6	7.42	7.1	7.11	6.05	5.92	9.9	5.66	9.0	4.07	3.97	0.75	0.1	1.54	1.27
MgO	9.1	3.67	4.51	1.99	7.28	8.33	0.72	4.96	4.98	2.4	3.38	7.47	6.24	2.38	3	6.86	3.3	4.41	1.46	1.46	0.19	0.04	0.43	0.45
CaO	9.5	9.24	7.9	5.73	7.5	10.4	3.6	9.8	9.56	5.26	5	9.2	7.45	7.78	9.9	6.44	7.02	4.01	6.71	4.49	0.96	0.45	1.49	2.35
MnO	0.15	0.25	0.17	0.09	0.16	0.21	0.03	0.19	0.14	0.1	0.1	0.13	0.15	0.12	0.08	0.15	0.11	0.12	0.07	0.11	0.03		0.03	0.04
Na_2O	3.02	3.26	3.47	5.86	2.9	2.49	5.41	3.13	2.43	3.98	4.87	2.58	2.54	3.36	3.27	2.78	3.26	3.47	4.69	3.42	4.16	7.7	5.16	5.29
K_2O	0.72	0.45	0.66	0.59	1.86	0.23	0.41	0.98	1.11	1.59	0.75	1.4	2.22	0.81	2.09	1.93	1.22	2.36	1.23	2.3	3.28	0.15	2.27	0.92
P_2O_5	0.13	0.38	0.22	0.27	0.1	0.02	0.05	0.21	0.1	0.19	0.18	0.12	0.18	0.17	0.08	0.06	0.12	0.26	0.16	0.17	0.08	0.08	0.04	0.1
LOI	1.78	1.56	1.29	1.22	3.75	2.26	0.85	2.29	1.96	3.19	2.76	2.03	1.91	4.06	3.67	3.87	2.26	6.02	1.96	2.19	1.07	0.27	3.01	0.98
Total	99.7	98.8	99.0	100.3	98.7	99.2	99.6	100.4	98.6	99.2	98.5	99.1	98.8	99.5	100.3	98.8	98.9	98.6	99.7	100.2	98.6	99.6	100.4	100.1
Ba	527	340	823	297	402	606	994	712	583	1780	926	364	695	73	265	1350	349	522	393	549	188	223	575	329
Be			2	2	2	2	1	1	1	1	1	1	2	2		2	1	2	1	1	1		1	2
Co	45	79	26	25	41	44	63	73	26	29	45	43	48	43	58	42	34.4	64	24.7	40	47	71	35	44
Cr				196	357	342			27		76	34			374		81		64	458	75	29	194	86
Cu			11	19	34	15	13		27	19	29						19		28	43				17
Ga	17.8	13.4	17.1	14.1	14.2	15	11.9	13	16.9	15.9	15.8	19	11.8	18.1	21.1	17.3	15	19.4	16.2	13.9	17.5	18	18.4	13
Hf	4.3	2.7	7.2	2.8	3.5	2.4	4	2.1	0.9	2.4	1.4	4.9	4.1	1.9	7.7	3.2	4.1	3.5	1.7	1.5	5.3	5.3	2.7	1.5
Nb	5.3	4.7	7.9	5.9	6.1	7.1	3.7	6.6	1.4	5.9		9.6	4.1	3.5	49.4	5.7	9.1	4.7		2.7	12	26.8	2.9	2.7
Ni		59		241	63	74					34	53		19	165		34		30	62	35		95	20
Pb	5.6						223									7	9	5				8		12
Rb	19	10	50	26	46	80	83	18	44	71	55	22	47	2	29	59	41	34	53	60	12	10	63	39
Sc	39	14	30	16	24	46	5	37	27	13	14	34	23	19	13	21	17	16	8	7	2	2	3	2
Sr	378	461	472	511	398	347	82	558	731	448	737	366	118	293	384	610	209	441	819	429	191	271	402	415
Ta	0.4	0.5	0.5	0.4	0.4	0.4	0.5	0.9	0.1	0.3		0.6	0.4	0.1	2.9	0.5	0.7	0.4		0.2	1.1	3.4	0.2	0.3
Th	3.3	13	8.3	2.4	4.3	8.1	6.2	3.1	1.4	2.3	0.4	3	6	0.1	3.7	9.2	5	1.2	0.3	2	1.9	2	1.2	5.5
Tl			0.2	0.2	0.2	0.3	0.5	0.1	0.3	0.5	0.3	0.2	0.2		0.2	0.3	0.2	0.2	0.4	0.3			0.3	0.2
U	1.2	3	2.1	0.7	1.3	3	2.3	0.8	0.6	1.4	0.2	0.9	2.1		1.9	3.6	1.2	1.5	0.1	0.7	1	2.5	0.4	1.1
V	187	58	249	80	128	302	27	249	154	89	120	165	144	127	140	310	113	144	67	55			9	
Y	19.4	9.4	27.7	19.8	22.9	24.4	16.9	6.8	7.4	19	8.9	49.6	26.9	44.8	32.8	10.8	20.9	12.4	9	12.4	50.9	64.8	16	13.4
Zn	42		45	40	47	65	677		37	59	54	94		82	118	42	46	39	34	60	57	50	76	59
Zr	175	8	282	100	140	70	150	75	35	105	55	175	160	50	325	120	155	145	70	51	200	195	108	50
La	19.7	24.8	44.8	14.2	18.2	18.5	16	16.4	8.8	18.7	6.9	14.2	20.6	5.8	35.6	35.8	31.6	9.7	5.2	10.8	12.2	17.2	8.2	10.5
Ce	36.7	37.6	81	28.4	37.5	40.7	31.7	27.7	15.3	36.6	13.1	35.7	38.9	21.1	72.7	62.3	62.5	17.5	11	21.7	33.9	47.5	16.8	21.6
Pr	4.5	4.3	9.4	3.6	4.9	5.4	3.5	2.8	1.8	4.5	1.6	4.7	4.6	4	9.3	6.3	6.7	2.2	1.4	2.6	5.1	6.6	2.2	2.5
Nd	15.9	12.4	31.1	13.1	18.4	20	12	8.05	6.31	16.6	6.35	19.3	16	194	34.6	21	23.7	8.6	6	9.9	21.7	28	8.6	9.1
Sm	3.6	2.17	6.3	3.27	4.5	4.28	2.61	1.43	1.43	3.69	1.7	5.66	3.53	6.19	8.19	3.54	5.1	2.17	1.52	2.39	6.7	8.55	2.32	2.13
Eu	1.1	0.36	1.53	1.12	1.31	1.22	0.48	0.44	1.13	1.38	0.77	1.94	0.72	1.65	3.17	1.11	1.33	1.12	0.69	0.79	2.12	2.93	1.26	0.81
Gd	4	2.12	6.43	3.72	4.56	4.47	2.75	1.38	1.6	4.11	1.84	7.34	3.77	7.72	9.01	3.05	4.84	2.41	1.79	2.45	8.14	10.4	2.8	2.46
Tb	0.6	0.27	0.87	0.56	0.69	0.62	0.42	0.19	0.21	0.56	0.27	1.3	0.61	1.24	1.19	0.36	0.69	0.35	0.27	0.38	1.36	1.76	0.44	0.35
Dy	3.3	1.51	4.91	3.34	3.84	3.57	2.58	1.09	1.27	3.26	1.6	8.04	3.71	7.53	6.3	1.82	3.75	1.97	1.65	2.13	8.36	10.8	2.67	2.09
Ho	0.7	0.32	1.06	0.73	0.84	0.8	0.61	0.24	0.28	0.71	0.34	1.87	0.91	1.7	1.21	0.36	0.75	0.45	0.34	0.44	1.9	2.39	0.59	0.47
Er	2.1	0.99	3.01	2.07	2.46	2.49	2.02	0.68	0.81	2.14	1	5.61	2.89	4.98	3.06	1.1	2.3	1.31	0.97	1.35	5.53	7.1	1.83	1.36
Tm	0.3	0.15	0.44	0.29	0.34	0.38	0.34	0.1	0.1	0.32	0.14	0.83	0.48	0.74	0.38	0.16	0.34	0.2	0.13	0.2	0.81	1.07	0.28	0.21
Yb	1.9	1.01	2.53	1.78	2.11	2.54	2.33	0.73	0.7	2	0.82	4.88	3.08	4.28	2.24	1.09	2.07	1.26	0.84	1.24	5.03	6.37	1.78	1.33
Lu	0.3	0.16	0.35	0.26	0.31	0.38	0.39	0.1	0.1	0.29	0.12	0.75	0.49	0.62	0.28	0.19	0.29	0.2	0.12	0.18	0.72	0.87	0.29	0.2
ΣREE	95	88	193	77	100	105	78	61	40	95	37	112	100	87	187	138	146	49	32	57	114	152	50	55
$(La/Lu)_n$	7.6	16.1	13.3	5.7	6.1	5.1	4.3	17	9.2	6.7	5.9	2	4.4	1	13.2	19.5	11.3	5	4.5	6.2	1.8	2	2.9	5.4
$(La/Sm)_n$	3.4	7.2	4.5	2.7	2.6	2.7	3.9	7.2	3.9	3.2	2.5	1.6	3.7	0.6	2.7	6.4	3.9	2.8	2.2	2.8	1.1	1.3	2.2	3.1
Eu/Eu*	0.9	0.5	0.7	1	0.9	0.9	0.5	0.95	2.3	1.1	1.3	0.9	0.6	0.7	1.1	1	0.8	1.5	1.3	1	0.9	0.95	1.5	1.1

Cum cumulative rocks, *Pl-dif* plagioclase-rich differentiates, *Di-grd* diorite to granodiorite, *Di-Grd* diorite to granodiorite, *Grd* granodiorite, *Lc* leucotonalite

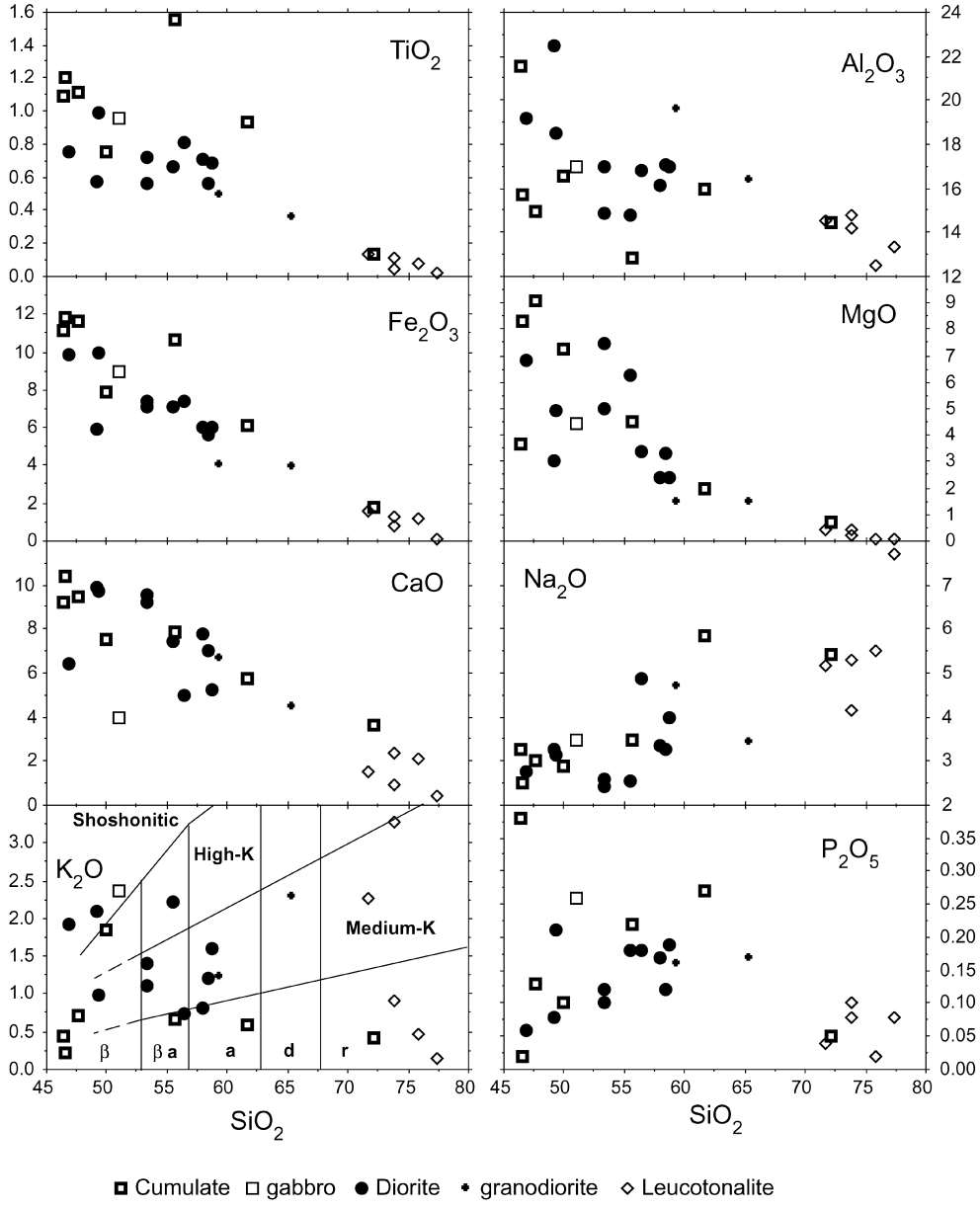

Fig. 10 Variation of the major oxides against SiO_2 for the diorites and related rocks of the Mérida Massif. The *dividing lines* in the SiO_2 vs. K_2O diagram are from Peccerillo and Taylor (1976)

deviate from the rest: these are samples BM51 and BM14 with distinctly more fractionated patterns [$(La/Lu)_n$= 18.3±1.8; $(La/Sm)_n$=6.8±06] and sample BM40 which, although less fractionated, is distinctly richer in REE (187 ppm). The fourth group, formed by the samples from the San Pedro area, presents also high REE contents (ΣREE=115±20 ppm), but nearly flat or even LREE depleted patterns [$(La/Lu)_n$=1.7±0.5; group D)].

On the NMORB-normalized trace elements plots (Sun and McDonough 1989), the samples studied exhibit features considered distinctive of subduction-related magmas (Pearce 1982; Wilson 1989; McCulloch and Gamble 1991, among others; Fig. 12). Most of them are enriched in strongly incompatible large-ion lithophile elements (LILE), with strong depletion in Nb and Ta relative to La and an enrichment in Pb over Ce (Fig. 12A, B, C). Only the diorites from the San Pedro area differ from these generic features, showing a less pronounced enrichment in LILE and greater similarity with the MORB compositions (Fig. 12D). It may be noted that some rocks included within the group C of cumulative diorites (notably, the REE-rich sample BM40) exhibit high Nb and Ta contents, actually more typical of alkaline series and that may reflect a change in the mantle-melting processes related to the origin of the intrusives.

Sm-Nd and Sr isotope results

Sm-Nd and Sr isotopic compositions of garnet-bearing diorite, leucodiorite, hornblendite and plagioclase-rich differentiates of the Mérida Massif are presented in Table 7. The Sr content of garnet-bearing diorite is substantially higher than that of the other rocks (ca. 590 and

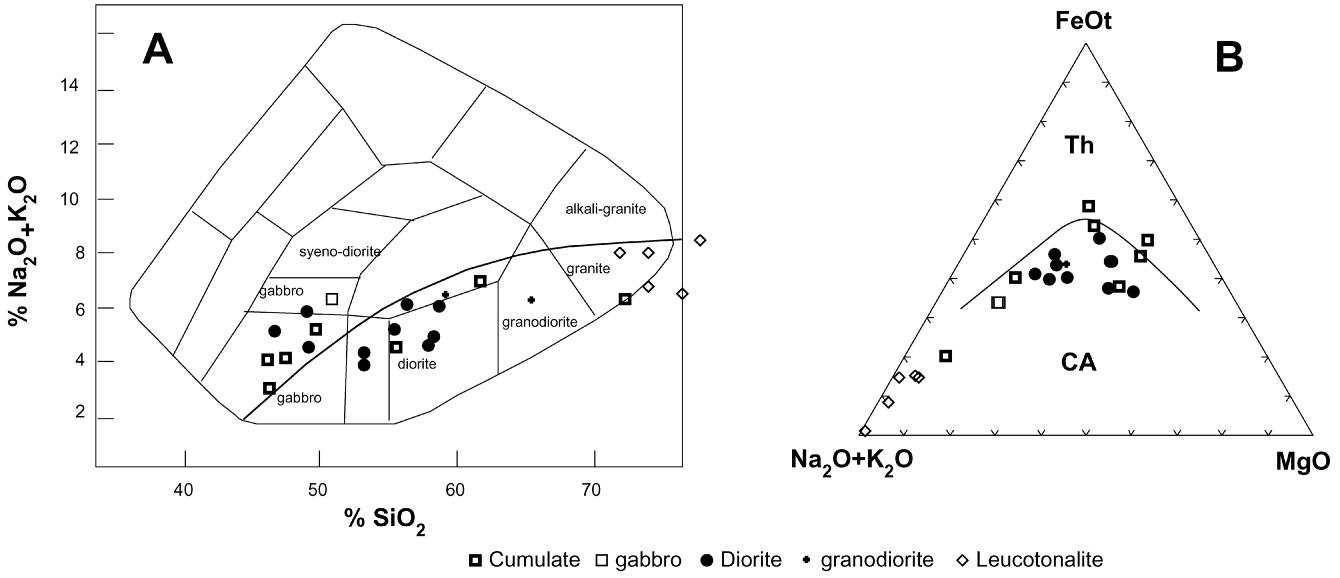

Fig. 11 **A** TAS diagram (after Cox et al. 1979, modified for plutonic rocks after Wilson 1989) showing the composition of igneous rocks from the Mérida massif. The *dividing line* between alkalic and sub-alkalic magama series is from Misyashiro (1978). **B** AFM diagram for the igneous rocks of Mérida. Separation of tholeiitic and calc-alkaline fields according to Irvine and Baragar (1971)

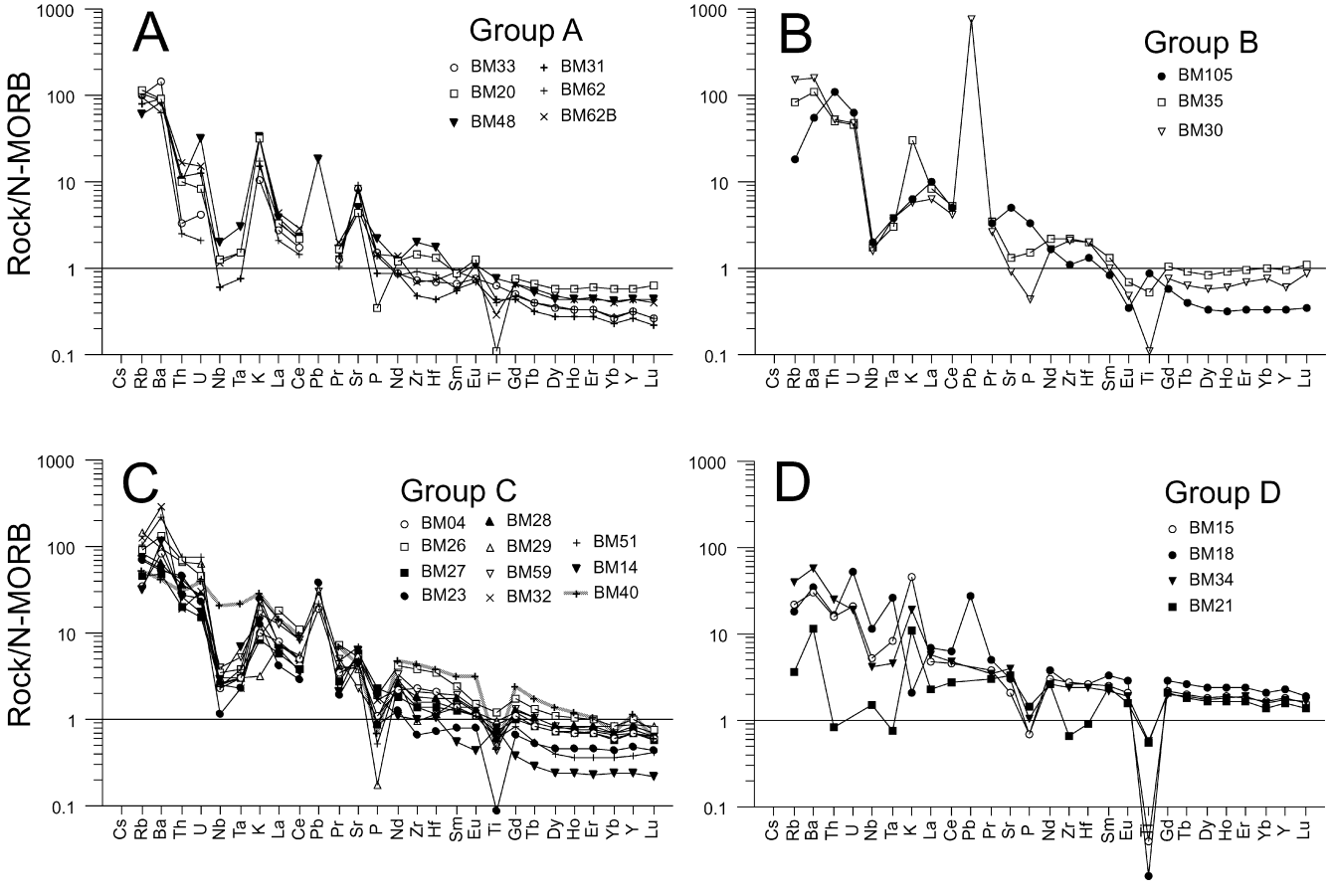

Fig. 12 Primitive mantle-normalized element distributions for the four groups distinguished of diorites and related rocks (cf. text) of the Merida Massif (normalizing factor after Sun and McDonough 1989)

Table 7 Whole rock Rb-Sr and Sm-Nd isotope data for diorites and related rocks of the Mérida massif

Sample	Rock type	Rb	Sr	$^{87}Rb/^{86}Sr$	$^{87}Sr/^{86}Sr$	Sri_{575}	ϵSr_{575}	Sm	Nd	$^{147}Sm/^{144}Nd$	$^{143}Nd/^{144}Nd$	ϵNd_0	ϵNd_{575}	T_{DM} (Ga)
BM105	Grt-bearing diorite	6.1	588	0.030	0.704014±5	0.70377	–0.66	1.53	6.05	0.1520	0.512588±5	–1.0	+2.3	1.13
MER1	Grt-bearing diorite							6.60	22.3	0.1789	0.512710±5	+1.4	+2.7	1.46
MER2	Grt-bearing diorite							5.29	21.5	0.1485	0.512579±7	–1.2	+2.3	1.09
BM27	Leucodiorite	11.4	278	0.119	0.705443±6	0.70447	9.3	8.6	29.8	0.1748	0.512699±5	+1.2	+2.8	1.15
BM4	Hornblendite	12.2	290	0.122	0.704781±4	0.70378	–0.45	2.34	7.96	0.1776	0.512697±6	+1.1	+2.5	1.11
BM30	Plagioclase differentiate	9.3	277	0.097	0.705424±5	0.70463	11.6	5.64	20.7	0.1676	0.512725±6	+1.7	+3.8	1.06

280 ppm, respectively). After age correction for in situ decay of ^{147}Sm and ^{87}Rb from 575 Ma, the initial $^{87}Sr/^{86}Sr$ ratios are similar within analytical error for all rock types: 0.7038 to 0.7046; likewise, the ϵNd_{575} values for diorites and related rocks have a limited range of +2.3 to +3.8. In all cases, the $^{87}Sr/^{86}Sr_i$ ratios are higher and the ϵNd values lower than those of present-day N-MORB (assumed 0.7020–0.7030 and +10, respectively) suggesting the participation of a component with higher $^{87}Sr/^{86}Sr$ and lower ϵNd ratios than those of mantle values in the genesis of these rocks. T_{DM} ages (De Paolo 1981; Table 7) point to a component bearing nonradiogenic Nd and thus favour a context of an active continental margin (or otherwise a great proportion of subducted sediments) rather than that of an island arc.

Discussion

Age of the igneous crystallization

U-Pb data obtained by two different methods on zircon fractions and single crystals from rocks of dioritic and granitic composition of the northern Ossa-Morena batholith show remarkable consistency. Considering the very subordinate degree of Pb loss and the lack of any inheritance, the age obtained of 577.6±0.6 Ma by ID-TIMS methods is thus interpreted to date the igneous crystallization of the dioritic intrusive of Mérida. Likewise, the age of 573±14 Ma by SHRIMP methods for the Valle de la Serena granite studied was obtained in typical magmatic oscillatory domains of constituent zircons and hence it is interpreted as the igneous crystallization age of the porphyritic granite. The Neoproterozoic ages reported here are among the oldest for igneous intrusives within the Ossa-Morena Zone, supporting the presence of Cadomian basement within the Iberian Massif.

Age of the metamorphic recrystallization

The status of the constituent garnet and the significance of Sm-Nd garnet-whole rock data in garnet-bearing rocks of mafic to intermediate composition like those studied here, have been the subject of ample discussion, notably in relation to the tectono-thermal evolution of the deep crust in arc regions (e.g., Kohistan; cf. Burg et al. 1998; Ringuette et al. 1998, 1999; Yamamoto and Nakamura 1996, 2000; Anczkiewicz and Vance 2000). In the end, the petrological-geochronological problem is largely centred on the nature of the garnets studied: magmatic, metamorphic or both. Likewise, assuming that the Sm-Nd garnet-whole rock ages are not *sensu stricto* cooling ages (controlled by the only process of volume diffusion), the fact that they be younger than the U-Pb zircon age would indicate that they certainly do not date the time of igneous emplacement, but that they may reflect a slow cooling or some overprinting. The question remains as to whether such cooling relates to a magmatic stage, to a magmatic-

metamorphic stage resulting of the igneous emplacement in a deep realm or just to a purely metamorphic overprint subsequent to an igneous, likely supracrustal, event. In principle, the petrographic, mineralogical and structural observations should allow us to provide an answer to those questions, although the answer might by no means be a simple one.

In the present case, the garnets from felsic to ultramafic rocks studied point to an extended history involving more than one period of growth. Traces of an initial stage of growth are best preserved in the Ca- and Mg-poorer cores of cm-size garnets rich in inclusions of plagioclase, zircon and ilmenite. Renewed garnet growth under significantly higher P conditions was responsible for the development of clear idiomorphic rims on those garnets and, most likely also, of limpid, small oriented garnets in the rock matrix with evidence of a peritectic origin (plagioclase enrichments around the garnets). Homogenization of the major element garnet compositions and P–T results indicate that T conditions above 750 °C prevailed during this late formation stage allowing for eventual garnet equilibration near the Sm-Nd closure temperature for moderate grain size and cooling rate (Ganguly et al. 1998). The Sm-Nd ages obtained of ca. 553.4– 555.9 Ma may thus be close to that of the metamorphic peak (Fig. 9B). These values were obtained after thorough leaching of the garnet fraction to prevent contamination by rare earth-bearing microinclusions and, while the difference of 2.5 Ma could reflect some disequilibrium between analysed minerals, they may be regarded as equivalent within error. Such an age around 553–556 Ma is in good agreement with previous Ar/Ar ages for muscovite and hornblende from the regionally metamorphosed associated metasediments and metabasites (Blatrix and Burg 1981; Dallmeyer and Quesada 1992) and is thus interpreted as a lower limit for the age of the pre-Variscan metamorphic imprint across the region. The slightly older ages of ca. 557–564 Ma are less precise and less reliable since they were obtained on unleached fractions. As for the significance of the oldest Sm-Nd age obtained, ca. 593±8 Ma, it will be discussed in relation to the Lu-Hf data.

The Lu-Hf system has the potential to provide a good geochronometer because of the refractory and relatively immobile behaviour of Lu and Hf during metamorphism and alteration. We have obtained an age of ca. 637±40 Ma for a whole rock-garnet pair from a garnet-bearing diorite of the Mérida Massif (Fig. 9E). Although rather imprecise an isochron due to the small difference in the Lu/Hf ratios of garnet and whole rock, this result overlaps within error the oldest Sm-Nd age of 593±8 Ma obtained on these rocks, pointing to an older period of garnet growth before the crystallization of zircon from the dioritic magma. Unfortunately, there is no direct field evidence for a regional metamorphic event prior to the magma emplacement dated at ca. 578 Ma, since the contacts of the intrusives with the host rocks are usually strongly tectonized. However, it may be inferred from their deep emplacement level (cf. petrology section) that the diorites were emplaced into a pre-existing medium- or even-high grade metamorphic pile. Although the age and duration of such regional metamorphic event cannot be assessed at Mérida, it is emphasized that an anatectic episode related to a regional metamorphic event at 600±13 Ma is documented some 100 km away, in southern sectors of the Ossa-Morena Zone (Lora del Rio anatectic dome; Ordóñez 1998). Also, if the older ages were the result of rotated mixing lines, that would imply that at the age of igneous emplacement (ca. 578 Ma) the garnet whole-rock tie-line should have a slope greater than zero, the garnet being older than 578 Ma, or the garnet contained inclusions bearing Nd and Hf more radiogenic than the magma—in summary, an inheritance phenomenon appears evident. Otherwise, one may also envisage that the rotation of the whole rock-garnet tie line be related not to the existence of a too radiogenic garnet but, on the contrary, to a diminution in the isotopic composition of the whole rock, resultant of a relatively late (by comparison with the crystallization of garnet cores) mixing with a less radiogenic ‘crustal melt’; this is perhaps a more realist hypothesis and, in any case, it does not involve the occurrence of older garnet. Whatever the case, the isotopic equilibrium between garnet and whole rock was not achieved, ensuing too old an age. Additional evidence for the possible incorporation of garnet-bearing metamorphic crust in the crystallizing dioritic magmas could be inferred from the geochemical data as discussed below.

Significance of the geochemical data

Most rocks studied from the Mérida area share chemical features suggestive of a convergent margin setting. The negative anomalies in Ti, Nb and Ta relative to REE are typical of subduction-related magmas, as are the distinctive arc signatures Zr/Nb, Ba/Nb and other elemental ratios shown for comparison on Table 8 (although some differences can be observed, as previously stated). On a whole, the trace element characteristics of the Mérida rocks (Tables 6 and 8) provide good evidence for the introduction of sedimentary material within the mantle region of provenance of the magmas, likely a mantle wedge, and reflect also large heterogeneities into the source area, although they can not exclude unequivocally the assimilation of crustal materials by ascending magmas. In addition, the REE features support the operation of different melting processes and conditions at the origin of the dioritic and related magmas. Thus, the Alange gabbros and the Don Álvaro tonalites have high (La/Sm)n and positive Eu/Eu* ratios, suggesting an amphibole-bearing source, whereas most other tonalites and granodiorites bear high (La/Lu)n ratios indicative of a garnet-bearing source.

The hornblendites are isotopically the most primitive rocks studied and may be considered as the closest approximation to a primary magma derived from the mantle wedge. When compared with the MORB compositions, those of hornblendites plot along the mantle array with

Table 8 Average of trace element ratios for N-MORB, Indian Ocean sediments, Mepari volcanism and rocks of the Merida Massif

	MORB	SA	SB	SC	Mepari	Mérida group A	Interval	Mérida group B	Interval	Mérida group C	Interval	Mérida group C	Interval
Zr/Nb	31.8	13.2	11.9	20.1	28.4	28.1	(37–19)	32.5	(41.0–17.3)	20.3	(35.7–9.8)	14.1	(18.4–7.3
Ta/Nb	0.06	0.08	0.06	0.09	0.1	0.07	(0.09–0.07)	0.11	(0.14–0.10)	0.08	(0.11–0.05)	0.08	(0.13–0.03)
Zr/Hf	36.1	30.6	35.8	36.1	41.0	38.7	(41.6–34.3)	35.7	(39.2–30.1)	37.0	(43.0–29.1)	34.1	(37.6–26.2)
Ba/Nb	2.7	98	6.8	21	146	232	(416–111)	170	(269–72)	121	(302–38)	21	(38–8.3
Th/Nb	0.05	0.90	0.40	1.20	2.0	0.60	(1.00–0.26)	1.97	(2.77–1.46)	0.9	(2.04–0.39)	0.14	(0.31–0.03)
Ce/Nb	3.2	7.9	3	4.8	10.4	7.1	(11.0–3.7)	8.7	(9.5–8.0)	7.0	(10.2–4.8)	3.6	(6.0–1.8)
Ba/Zr	0.09	7.4	0.8	1.0	4.9	9.9	(17.5–3.6)	5.0	(6.6–4.2)	6.8	(17.3–2.2)	1.4	(2.1–0.9)
Th/Zr	0.002	0.07	0.04	0.06	0.07	0.02	(0.04–0.004)	0.08	(0.16–0.04)	0.05	(0.12–0.02)	0.01	(0.02–0.002)
Ce/Zr	0.1	0.6	0.36	0.24	0.4	0.3	(0.4–0.1)	0.3	(0.5–0.2)	0.4	(0.6–0.2)	0.3	(0.4–0.2)
Ce/Pb	25	3.4	3.9	2.2	2.1	3.2	(3.2–3.2)	0.1	(0.1–0.1)	6.2	(6.9–1.9)	5.8	(5.8–5.8)
Ba/La	2.5	27.3	5.9	9.3	28	75	(135–51)	37	(62–14)	34	(95–11)	17	(25–13)
Th/U	2.6	6.6	8.1	3.7	4.9	2.3	(3.0–0.8)	3.3	(4.3–2.7)	3.3	(5.0–1.6)	2.0	(3.3–0.8)

N-MORB: Sun and McDonough (1989); Indian Sediments: Gasparon and Varne (1998), Plank and Langmuir (1998); Mepari volcanism: Gertisser and Keller 2003

higher $^{87}Sr/^{86}Sr$ ratio and lower ϵNd values. This implies a compositional gap between the hypothetical MORB source and the melts issued. Such a gap may be observed in present-day island-arc settings such as the eastern Sunda or northeastern Banda arcs, among others. In northeastern Banda, for instance, the lavas show a wide range in silica contents (SiO_2=51–70%) with a normal arc signature of $^{87}Sr/^{86}Sr$=0.7045–0.7055 and ϵNd=+5 to +1, whereas those in the extreme southeast are essentially andesites with $^{87}Sr/^{86}Sr$=0.7065–0.7083 and ϵNd=+2 to +4, suggesting assimilation of crustal component at shallow levels or contamination by subducted continental material (Vroon et al. 1993; Hoogewerff et al. 1997).

The strong positive correlation between the silica contents and the Sr and Nd isotope composition, suggesting an assimilation and fractional crystallization (AFC) process or, alternatively, different melting regions with variable input of sedimentary component added to the mantle wedge. Most chemical features of the Mérida rocks are comparable to those typical of medium- to high-K volcanic rocks elsewhere (e.g., Mepari in Java; cf. Table 8) that argue for variable source enrichment related to the fluid flux from the slab. Therefore, a slightly higher degree of partial melting induced by a higher water flux from the slab may account for lower abundances of immobile trace elements (Gertisser and Keller 2003). Indeed, the rocks studied are substantially enriched in continental crust-like components when compared with calc-alkaline series elsewhere within the same geotectonic zone (e.g., the Sierra de Córdoba andesites, Pin et al. 2002). Significant contamination during ascent was also suggested through the Sm-Nd and Lu-Hf dating of apparently garnet relicts in the dioritic rocks. While the final result is a tendency towards isotopic and trace-element compositions approaching those of the metasediments, it may be noted that some samples, e.g., those from the San Pedro area (group D in Fig. 12), have preserved MORB-like REE features that substantiate the complexity of the process.

Gertisser and Keller (2003) proposed a model to reconcile isotope data pointing to a variable and restricted (1–10%) source enrichment by subducted sedimentary materials, and geochemical data more consistent with variable source melt degree (with minor assimilation processes). In this sense, we have used the REE compositions for modelling the melting process of a mantle source to produce the Mérida diorites and related rocks. The concentrations at the source are assumed similar to those of a modified MORB (represented by sample BM34). The trace element partition coefficients used for each mineral are shown in Table 9. The relatively low normalized values for $(Yb)_n$ suggest a garnet-bearing source for most samples, while the high $(La/Sm)_n$ ratios are indicative of amphibole. That is, the patterns of the studied samples suggest the presence of minerals that concentrated medium REE, as well as heavy REE, in the mantle residue. Figure 13 shows the results obtained for the modelled melting processes in terms of melt fraction (ranging from F=0.1 to F=0.65) and residual assemblages of the sub-

ducting slab. The relatively enriched samples BM50, BM14 and, particularly BM40 with OIB affinity, have been excluded from the model calculations. It may be observed that garnet and amphibole are the main minerals constituting the residual assemblages, while others such as olivine, orthopyroxene, clinopyroxene and plagioclase form also at times substantial amounts of these residua. The results of these models can be interpreted as indication of a variable degree of melting (related perhaps to different water influx from the subducting slab), and/or different pressure conditions as reflected by the variable amount of garnet in the modelled residua.

Table 9 Mineral/melt distribution coefficients for basaltic liquids used in the modeling

Ol[a]	Opx[a]	Cpx[b]	Grt[c]	Pl[b]	Hlb[b]	
La	0.007	0.02	0.06	0.001	0.19	0.54
Ce	0.006	0.02	0.09	0.007	0.11	0.84
Nd	0.006	0.03	0.23	0.026	0.09	1.34
Sm	0.007	0.05	0.45	0.10	0.07	1.80
Eu	0.007	0.05	0.47	0.24	0.44	1.56
Gd	0.010	0.09	0.56	0.68	0.07	2.02
Dy	0.013	0.15	0.58	1.94	0.06	2.02
Er	0.026	0.23	0.58	4.70	0.06	1.74
Yb	0.049	0.34	0.54	6.17	0.06	1.64
Lu	0.045	0.42	0.51	6.95	0.05	1.56

[a] Fujimaki et al. 1984
[b] Arth 1976
[c] Irving and Frey 1978

Geodynamic implications

The occurrence of a major Cadomian orogenic episode in the Ossa-Morena Zone, as was first proposed by Eguíluz and Ramón Lluch in 1983, is nowadays accepted by most authors working on this area of the Iberian Massif (cf. Eguíluz et al. 2000; Murphy et al. 2002 and references therein). Though an interpretation of this sector in terms of an island-arc setting during the Cadomian orogeny is generally agreed upon, the position and dip direction of the alleged oceanic subduction has been controverted. In the first models (e.g., Eguíluz and Ábalos 1992), it was assumed that the proposed contact between the Ossa-Morena and Central-Iberian Zones, following approximately the Variscan magmatic alignment of the Los Pedroches batholith (Julivert et al. 1972), would represent the Cadomian suture line, with the Cadomian ocean having been subducted beneath the Ossa-Morena Zone in a relative position quite similar to the present-day one. In that model, the Badajoz-Córdoba blastomylonitic domain was interpreted as a marginal basin, while the significance of the northern OVPR domain remained uncertain.

Detailed correlations between the various units recognized within the Ossa-Morena Zone and equivalent ones in the type localities of Cadomia (northern Armorican Massif) moved to a new and somewhat different model (e.g., Eguíluz et al. 1995, 2000). It was then assumed that the arc, which during the Neoproterozoic-Cambrian would form in the Ossa-Morena zone, was originally situated to the west of its present position and had rotated anticlockwise. The Cadomian ocean (Proto-Thetys, cf. Stampfli et al. 2002) would thus be subducted beneath this zone involving an important left-lateral component. There were no traces of continental collision or suture left, but only a few indices of the possible Cadomian subduction plane preserved on the northern edge of the OVPR domain (garnet-bearing rocks of Mérida and equivalent). Nonetheless, the large amount of dioritoids and related volcanic and volcanoclastic rocks cropping out in the massifs of Mérida, Oliva de Mérida, Palomas, Peraleda, etc. within that domain (Fig. 2), rather

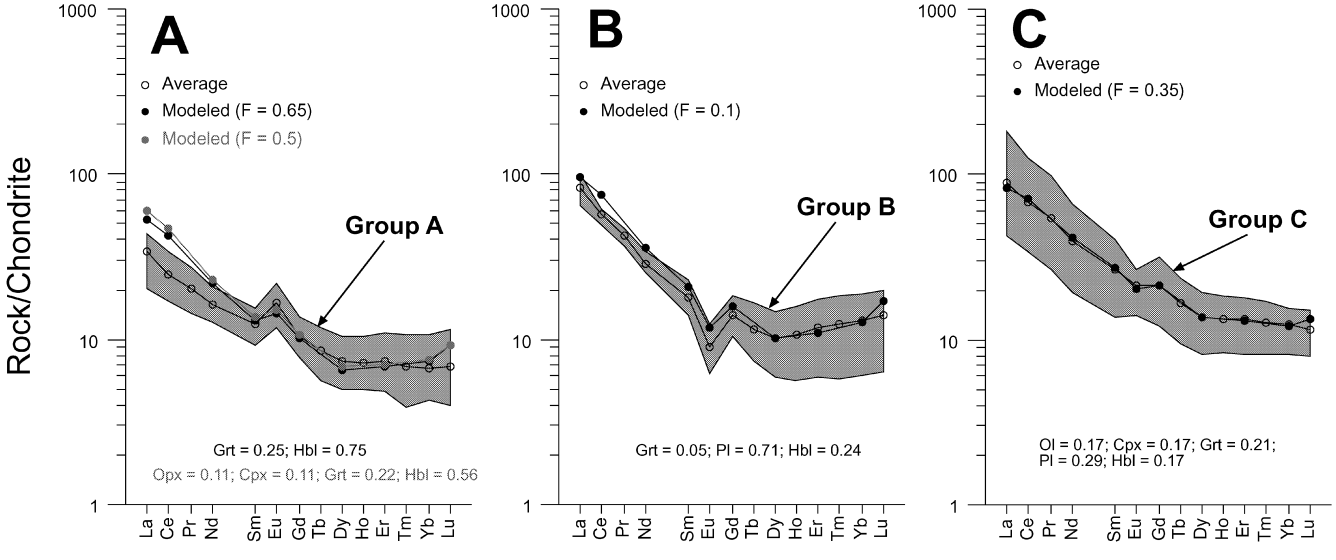

Fig. 13 Chondrite-normalized REE distribution for diorites and related rocks of the Merida Massif. *Shaded area*: compositional field for each group distinguished (cf. text). *Open symbols*: average of group composition. *Closed symbol*: calculated model. The composition of the calculated residue is given for each group

pointed to the foundations and mid- to supracrustal areas inside the constituent island arc. The limit between the Ossa-Morena and Central-Iberian Zones was considered to lie along a mainly strike-slip accident (San Pedro de Mérida-Montoro thrust fault, Fig. 2) corresponding to the outer limit of the arc region. Left-lateral movement parallel to the border between the intervening zones would continue through the Paleozoic until these reached its present position during the upper Carboniferous. The Badajoz-Córdoba shear zone was interpreted as an intra-arc basin closed during terminal episodes of the Cadomian cycle as late as 500–480 Ma (Ordóñez 1998), likely in relation to the anticlockwise rotation and induced by the expanding rift process that affected the whole region since the late Cambrian.

In both models, the migmatitic cores like those of Monesterio, Pintado, Mina Afortunada, etc., particularly conspicuous in southern Ossa-Morena areas, were considered to be the result of a major process of partial melting caused by the collapse of a moderately thickened crust.

On the other hand, it has been recently postulated that the Ossa-Morena Zone and related sectors of Cadomia evolved from a subduction-related arc growth stage near the Gondwana margin at ca. 600 Ma to a position close to the Central-Iberian Zone at ca. 500 Ma through an essentially transcurrent regime that involved several thousands of km of displacement (Fernández Suárez et al. 2002; Gutiérrez-Alonso et al. 2003). The model, based upon the apparent lack of Meso-Proterozoic components within constituent zircons of the Neoproterozoic Serie Negra and equivalent units from Brittany must however be handled with care since, as shown by Ordóñez (1998), albeit not abundant, inner cores of zircons from the Montemolín section of the Serie Negra yield concordant $^{206}Pb/^{238}U$ ages around 1.5 Ga.

Notwithstanding, the new data presented in this contribution concerning the abundant remnants of arc-type magmatism in northern Ossa-Morena sectors, together with the petrological and structural data gathered in the last years on the same region (Bandrés et al. 2002) permit us to update and refine the geodynamic model for this area which, in general terms, appears comparable to those proposed for other massifs of the Cadomian-Avalonian belt. A possible sequence of geodynamic scenarios and temporal evolution along several phases whose duration is constrained by available radiometric dating could be as in the following section.

Arc-growth and early metamorphic stages

During the Neoproterozoic III, a volcanic arc would develop by south-eastward oblique subduction beneath the western border of Gondwana. The arc was formed upon an active margin generating plutonic and volcanic rocks; the latter being intercalated with clastic sediments and occasionally phthanitic rocks. The mafic components would correspond to metabasalts and volcanoclastic sequences such as the precursors of the Montemolín amphibolites in southern Ossa-Morena, the Badajoz-Córdoba Shear Zone metabasites (protoliths dated at ca. 610 Ma; Schäfer 1990) and the gabbro-diorites to the north and south of this zone similar to those of the Mérida-Montoro alignment studied here that emplaced around ca. 580 Ma. Towards the south, in the present coordinates, of this formerly active zone, that is towards the old continent, reworked sediments of the Neoproterozoic Serie Negra, including some serpentinite slabs related to the arc building (Calzadilla de los Barros), were accumulated. In fact, the oldest metamorphic rocks preserved come from that continental realm. These are the high-grade gneisses of Lora del Rio which formed in a convergent regime (Apraiz 1998; Apraiz and Eguíluz 2001) at ca. 600 Ma (Ordóñez 1998). The new Sm-Nd and Lu-Hf results for garnet whole-rock pairs obtained in this study suggest that the first episodes of arc building in northern Ossa-Morena might have started at nearly the same time.

Tectonic shortening and thickening

As a result of the amalgamation of the arc and continental terranes and/or of the collision with an eventual oceanic ridge, the whole region was subject to a process of tectonic shortening and thickening accompanied by metamorphism and major deformation. Strike-slip faulting and coeval thrusting in relation to these events has been dated by cross-cutting plutons and cooling metamorphic ages between ca. 560 and 550 Ma throughout the whole Ossa-Morena region (e.g., Bellon et al. 1979; Blatrix and Burg 1981; Dallmeyer and Quesada 1992; Quesada and Dallmeyer 1994). Medium- to high-grade metamorphic conditions like those documented and dated in this study for the Mérida area would be related to this stage reflecting the tectono-thermal evolution within lower sections of the outermost arc domain.

Orogenic collapse

Collapse of the Cadomian orogenic belt would have started a phase of crustal extension that resulted in the ascent and exhumation of migmatitic cores along the edges of an incipient intra-arc basin. Two main gneiss dome belts related to this event have been identified in the Ossa-Morena Zone: (1) to the south, a belt comprising the Garrotal, Monesterio and Assumar migmatitic cores, and (2) along the Badajoz-Córdoba Shear Zone, the anatectic areas of Mina Afortunada, Fuente Obejuna and Argallón-Llera (Azuaga gneisses). Other poorly known cores, like Évora, could also probably be related to this episode. The age of this phase is constrained between that of the migmatites and associated granites dated at ca. 530 Ma (e.g., Monesterio and Mina Afortunada; Ochsner 1993; Ordóñez 1998) and the late-orogenic volcanics of the Malcocinado Formation established around 525–515 Ma (Ordóñez 1998).

Late orogenic and post-Cadomian evolution

An event of calc-alkaline to shoshonitic volcanism concomitant of uplift and the widespread erosion of both volcanics and basement marks the final stages of the arc evolution and the approach to the end of the orogenic activity. This volcanism is represented for instance by the Malcocinado and equivalent San Jerónimo and Bodonal andesite to rhyolite formations (Pin et al. 2002 and references therein) whose age, progressively younger towards the south of the region, has been established around 525–515 Ma (Ordóñez 1998).

Crustal relaxation and thinning, subsequent to the collisional stages, evolved into a period of generalized rifting during Cambrian-Ordovician times across the formerly active orogenic areas. The rifting phase was responsible for the formation of early Paleozoic sedimentary basins and the emplacement of igneous rocks with alkaline affinity close to the anatectic core areas in the 510–475-Ma-age interval (Priem et al. 1970; Lancelot and Allegret 1982; García Casquero et al. 1985; Ochsner 1993).

Conclusions

Dioritic to leucotonalitic intrusives within northern sectors of the Ossa-Morena Zone were emplaced into lowermost terms of a Precambrian metavolcanic and metasedimentary sequence. The H_2O-rich magmas evolved by fractional crystallization of amphibole and plagioclase producing a variety of cumulate types together with minor amounts of granodiorite and granitic rocks. Cumulate products are amphibole-rich gabbros to hornblendites associated often with plagioclase-rich rocks. The crystallization of diorites and cumulate rocks at depth likely involved the assimilation of metamorphosed crust, as inferred from the geochemical data and the indices of garnet older than the magmatic zircon in some of these rocks. Major and trace element composition of the diorites and related rocks, including Sr and Nd isotope data for selected samples, allow the characterization of the whole igneous sequence as belonging to a calc-alkaline series likely formed in relation to an immature arc setting. The age of crystallization of the dioritic and granitic magmas has been established between ca. 570 and 580 Ma by U-Pb dating of constituent zircons using ID-TIMS and SHRIMP methods. Renewed garnet growth in some diorites may be interpreted as a subduction-related tectono-thermal overprint within the arc environment. The large idiomorphic garnets of these rocks retain evidence of a two-stage growth process and, in cases, prograde major element zonation. The Sm-Nd ages around 555 Ma for internal isochrons are interpreted as dating cooling through 700–800 °C following magmatic crystallization and high-grade amphibolite to granulite facies metamorphism. Older Sm-Nd and Lu-Hf ages between ca. 593 and 637 for garnet whole-rock pairs indicates the possibility of earlier episodes of arc building whose products were subsequently incorporated into the main orogen-building process. The northern Ossa-Morena composite batholith and related metamorphic units have been tectonized and dismembered in the course of subsequent low-grade events during the final stages of the Cadomian orogeny and the Variscan cycle, the latter equally affecting the overlaying discordant post-Tremadoc series.

It is proposed that the northern Ossa-Morena igneous and metamorphic units described here represent a well-preserved segment of the island arc that evolved in Neoproterozoic times along the western border of Gondwana to conform the Cadomian-Avalonian Massifs that shaped the basement of the Hercynian realm. Taking into account the available geochronological data for the study area and the nearby Badajoz-Córdoba belt, it may be assumed that a major episode of arc building likely occurred along the 600–575-Ma interval. Accretion- or ridge collision-related metamorphism caused the principal recognizable medium- to high-pressure tectono-thermal event at ca. 555 Ma. Left-lateral slip appears to have been present along most of the tectonic evolution of this area. In turn, extension-related metamorphism and deformation of the previous moderately thickened crust are only recorded by anatectic core complexes to the south of the area studied. Likewise, further extension leading to the Cambrian–Ordovician rifting and Hercynian Basin evolution are best preserved in the central and southern Ossa-Morena sectors.

The evolutionary model presented above gives a consistent picture of the geological history of the Ossa-Morena Zone through the late Neoproterozoic up to the Lower Paleozoic. A reconstruction of the Cambrian Paleogeography along the European Cadomian foldbelt appears now possible, although more stratigraphical constraints are needed. Yet, it is clear that a number of problems remain unsolved, in particular regarding specific aspects of the regional tectonic evolution and precise timing of the different processes involved. There is not a definite explanation, for instance, for the process of amalgamation of the Ossa-Morena and Central-Iberian Zones; neither the geometry nor the tectonic imprint of this process in the latter zone are well understood at present. The significance in terms of lithospheric evolution of the complex tectonics and the geochronological pattern for the Badajoz-Córdoba band is equally unclear, although a continuous and many times protracted evolution could be imagined. Other questions that should certainly be addressed in future research are the so far poorly known relationships, if any, between the basements of the Ossa-Morena and South-Portuguese Zones.

Acknowledgments Financial support by Spanish MCYT (MAT2000–142, BTE20001-71 and BTE20003-3823) and French-Spanish cooperation "Picasso" (1997, 1998) grants is acknowledged. This manuscript is a contribution to IGCP 453. The authors are grateful to Dr. B. Ábalos for helpful discussions on the structural and petrological features of the study area.

Appendix

Analytical techniques

Whole-rock major and trace element analysis: Major (wt.%) and trace element (μg/g) concentrations were measured by simultaneous ICP-AES at the University of Bilbao following procedures described by Cantagrel and Pin (1984) and Pin and Joannon (1997). Total iron is given as Fe_2O_3. Analytical uncertainty for trace elements is estimated as 10% or better.

Isotopic analysis: Isotope dilution thermal ionisation mass spectrometry (ID-TIMS) U–Pb analyses were performed at the CNRS, Clermont-Ferrand on the least magnetic (2° forward and side tilt at 2.2 A using a Frantz Isodynamic magnetic barrier separator), mechanically abraded (Krogh 1982), and crack-free zircon grains. Zircon dissolution, chemical separation of U and Pb, and isotope analyses were carried out according to methods described by Paquette and Pin (2001). The U and Pb isotopes were analysed on a VG Sector 54–30 mass spectrometer in multi-collector static mode. The isotopic ratios are corrected for mass discrimination (0.1±0.015% per amu for Pb and U), isotopic tracer contribution and analytical blanks: 10 pg for Pb and 1 pg for U. Initial common Pb is determined for each fraction in using the Stacey and Kramers (1975) two-step model. Data errors (2σ) of the zircon fractions and discordia lines were calculated using the PBDAT 1.24 and Isoplot/Ex 2.49b programs (Ludwig 1993, 2001).

Minerals for SHRIMP U-Pb isotopic analyses were hand-picked from defined sieve 0.35 mm and magnetic separator. Zircons were separated using a magnetic drum separator, a Frantz isodynamic separator and heavy liquids. The zircons selected are mounted in epoxy and polished until an equatorial section is reached, the zircons were studied under back-scatter electronic microscope with a cathodoluminiscence device at the Metallforschung Institut, ETH Zürich. The same mount is used for in situ ion-microprobe analyses (SHRIMP-I and II, Sensitive High Resolution Ion Micro Probes) carried out at ANU (Australian National University) in Canberra, Australia. For a full description of the ion-microprobe technique and data acquisition we refer to Compston et al. (1984, 1986). All U-Pb ages are referenced to a $^{206}Pb/^{238}U$ value of 0.0928 (equivalent to 572 Ma) for the standard zircon used from a pegmatite from Sri Lanka (SL-13). The U/Pb data are presented in a concordia diagram (Wetherill 1956, 1963), where ellipses are plotted with 1σ error. All the data presented in the concordia were corrected for the common lead using the ^{208}Pb correction method.

Approximately 0·1 g of whole rock, spiked with ^{150}Nd-^{149}Sm mixed tracer solution, was used for Sm-Nd and Sr analyses. Sample dissolution, chemical separation of Sr, Sm and Nd and isotope analyses was performed following methods described by Pin and Santos Zalduegui (1997). Procedure blanks for Sr and Nd are typically below 50 pg. One garnet fraction of sample MER105 was leached prior to dissolution following a two-step procedure involving 1 ml of cold concentrated HF for 1 h followed by 7 N HNO_3 and 6 N HCl on a hot plate for 15 h. Sm-Nd and Sr isotope analyses were done at the University of the Basque Country using a Finnigan MAT262 on a static multicollection with a $^{143}Nd/^{144}Nd$=0. 511844±13 (2σ, n =18) value for La Jolla standard and $^{87}Sr/^{86}Sr$=0.71025±4 (2σ, n =33) for the Sr-standard NBS-987. Analytical uncertainty was estimated to be ± 0.2% on the $^{147}Sm/^{144}Nd$ ratio and 0.0016% on $^{143}Nd/^{144}Nd$.

Hf isotopes were measured with a multiple-collector inductively coupled plasma mass spectrometer (MCICP-MS) at the Ecole Normale Supérieure de Lyon. Samples were processed using a new sample digestion and Lu-Hf separation scheme, involving fusion with a LiBO2 fluxing agent and one extraction chromatography column based on diamyl amylphoshonate (DAAP). Typical Hf and Lu blank/sample ratios were negligible. The ^{176}Lu decay constant of Scherer et al. (2001) was used in the Lu-Hf age calculations with Isoplot.

Microprobe analysis: Mineral analyses were done using an automatic Cameca SX50 microprobe equipped with three spectrometers at the University of Oviedo (Spain). Operating parameters included a 10-s-counting time (peak), a c. 10 nA beam current and a 15 kV accelerating voltage. Calibration was against BRGM (French Geological Survey) standard minerals, and the ZAF correction procedure was used. Table 1 presents a selection of analytical data with additional details on structural formulas and Fe^{3+} estimates.

References

Ábalos B (1992) Variscan shear-zone deformation of late Precambrian basement in SW Iberia, implications for circum-Atlantic pre-Mesozoic tectonics. J Struct Geol 14:807–823

Ábalos B, Díaz Cusí J (1995) Correlation between seismic anisotropy and major geological structures in SW Iberia: a case study on continental lithosphere deformation. Tectonics 14:1021

Anczkiewicz R, Vance D (2000) Isotopic constraints on the evolution of metamorphic conditions in the Jijal-Patan complex and the Kamila Belt of the Kohistan arc, Pakistan Himalaya. In: Khan MA, Treloar PJ, Searle MP, Jan MA (eds) Tectonics of the Nanga Parbat Syntaxis and the Western Himalaya. Geol Soc Lond Spec Publ 170:321–331

Apalategui O, Borrero JD, Higueras P (1983) División en grupos de rocas en Ossa-Morena oriental. Temas Geol Min 7:73–80

Apalategui O, Contreras F, Jorquera A, Villalobos M, Eguíluz L (1988) Hoja 1:50.000, nº 804 (Oliva de Mérida), Mapa Geológico Nacional (MAGNA). Instituto Geológico y Minero de España, Madrid

Apraiz A (1998) Geología de los macizos de Lora del Río y Valuengo (Zona de Ossa-Morena). Evolución tectonometamórfica y significado geodinámico. PhD Thesis, Univ País Vasco, Bilboa, Spain, pp 1–575

Apraiz A, Eguíluz L (2001) Hercynian tectono-thermal evolution associated with crustal extension and exhumation of the Lora del Río metamorphic core compex (Ossa-Morena Zone, Iberian Massif, SW Spain). Int J Earth Sci 91:76–92

Arth NT (1976) Behaviour of trace elements during magmatic processes-a summary of theoretical models and their applications. US Geol Sur J Res 4:41–47

Bandrés A, Eguíluz L, Gonzalo JC, Carracedo M (1999) El macizo de Mérida, un arco volcánico cadomiense reactivado en el Hercínico. Geogaceta 25:27–30

Bandrés A, Eguíluz L, Gil Ibarguchi JI, Palacios T (2002) Geodynamic evolution of a Cadomian arc region: the northern Ossa-Morena Zone, Iberian Massif. Tectonophysics 352:105–120

Bellon H, Blachère H, Crousilles M, Deloche Ch, Dixsaut C, Hertrich B, Prost-Dame V, Rossi P, Simon D, Tamain G (1979) Radiochronologie, évolution tectono-magmatique et implications métallogéniques dans les Cadomo-variscides du Sud-Est Hespérique. Bull Soc Géol Fr 21:113–120

Blatrix P, Burg JP (1981) $^{40}Ar/^{39}Ar$ Dates from Sierra Morena (southern Spain): Variscan metamorphism and Cadomian orogeny. Neues Jahrb Miner Abh 10:470–478

Burg JP, Bodinier JL, Chaudhry S, Hussain S, Dawood H (1998) Infra-arc mantle-crust transition and infra-arc mantle diapirs in the Kohistan Complex (Pakistani Himalaya): petro-structural evidence. Terra Nova 10:74–80

Cantagrel F, Pin C (1984) Major, minor and rare earth elements determination in 25 standards by inductively coupled plasma-atomic emission spectrometry. Geostat Newslett 18:123–138

Castro A (1988) Los granitoides deformados de la banda del Guadámez (La Serena, Badajoz). In: Bea F, Carnicero A, Gonzalo JC, López Plaza M, Rodríguez Alonso MD (eds) Geologia de los granitoides y rocas asociadas del Macizo Hespérico: Libro homenaje a L.C. García Figuerola. Rueda, Madrid pp 413–426

Compston W, Williams IS, Meyer C (1984) U-Pb geochronology of zircons from lunar breccia 73217 using a sensitive high mass-resolution ion microprobe. J Geophys Res 89:(B):525-534

Compston W, Kinny PD, Williams IS, Foster JJ (1986) The age and Pb loss behaviour of zircons from the Isua supracrustal belt as determined by ion microprobe. Earth Planet Sci Lett 80:71–81

Cox KG, Bell JD, Pankhurst RJ (1979) The interpretation of igneous rocks. Allen and Unwin, London, 450 pp

Dale J, Holland T, Powell R (2000) Hornblende–garnet–plagioclase thermobarometry: a natural assemblage calibration of the thermodynamics of hornblende. Contrib Mineral Petrol 140:353–362

Dallmeyer RD, Quesada C (1992) Cadomian vs. Variscan evolution of the Ossa-Morena Zone (SW Iberia): field and $^{40}Ar/^{39}Ar$ mineral age constraints. Tectonophysics 216:339–364

De Paolo D (1981) Neodymium isotopes in the Colorado Front Range and crust-mantle evolution in the Proterozoic. Nature 291:193–196

D'Lemos RS, Strachan RA, Topley CG (eds) (1990) The Cadomian Orogeny. Geol Soc London Spec Publ 51:1–423

Droop GTR (1987) A general equation for estimating Fe^{3+} concentrations in ferromagnesian silicates and oxides from microprobe analyses, using stoichiometric criteria. Mineral Mag 51:431–435

Eckert JO Jr, Newton RC, Kleppa OJ (1991) The ΔH of reaction and recalibration of garnet–pyroxene–plagioclase–quartz geobarometers in the CMAS system by solution calorimetry. Am Mineral 76:148–160

Eguíluz L (1988) Petrogénesis de rocas ígneas y metamórficas en el Anticlinorio Burguillos-Monesterio, Macizo Ibérico Meridional. PhD Thesis, Univ País Vasco, Bilboa, Spain, pp 1–694

Eguíluz L, Ábalos B (1992) Tectonic setting of Cadomian low-pressure metamorphism in the central Ossa-Morena Zone (Iberian Massif, SW Spain). Precambr Res 56:113–137

Eguíluz L, Ramón Lluch R (1983) La estructura del sector central del dominio de Arroyomolinos, Anticlinorio Olivenza-Monesterio, Ossa Morena. Stud Geol Salamanca 18:171–192

Eguíluz L, Apraiz A, Ábalos B, Martínez-Torres LM (1995) Evolution de la zone d'Ossa Morena (Espagne) au course du Protérozöique supérieur: corrélations avec l'orogène cadomien nord armoricain. Géol Fr 3:35–47

Eguíluz L, Gil Ibarguchi JI, Ábalos B, Apraiz A (2000) Superposed Hercynian and Cadomian orogenic cycles in the Ossa-Morena Zone and related areas of the Iberian Massif. Geol Soc Am Bull 112:1398–1413

Evensen MM, Hamilton PJ, O'Nions RK (1978) Rare earth abundances in chondritic meteorites. Geochim Cosmochim Acta 42:1199–1212

Fernández Suárez J, Gutiérrez-Alonso G, Jeffries TE (2002) The importance of along-margin terrane transport in northern Gondwana: insights from detrital zircon parentage in Neoproterozoic rocks from Iberia and Brittany. Earth and Planetary Science Letters, 204, 75-88

Fujimaki H, Tatsumoto M, Aoki K (1984) Partition coefficients of Hf, Zr, and REE between phenocrysts and groundmasses. Proceedings of the 14th Lunar Planetary Science Conference, Part 2. J Geophys Res 89(B):662–672

Ganguly J, Tirone M, Hervig RL (1998) Diffusion kinetics of samarium and neodymium in garnet, and a method for determining cooling rates of rocks. Science 281:805–807

García Casquero JL, Boelrijk NAIM, Chacón J, Priem HNA (1985) Rb-Sr evidence for the presence of Ordovician granites in the deformed basement of the Badajoz-Córdoba Belt, SW Spain. Geol Rundsch 74:379–384

Gasparon M, Varne R (1998) Crustal assimilation versus subducted sediment input in west Sunda arc volcanics: an evaluation. Mineral Petrol 64:89–117

Gertisser R, Keller J (2003) Trace element and Sr, Nd, Pb and O isotope variations in medium-K and high-K volcanic rocks from Mepari Volcano, Central Java, Indonesia: evidence for the involvement of subducted sediments in Sunda arc magma genesis. J Petrol 44:457–489

Gonzalo JC (1987) Petrología y estructura del Basamento en el área de Mérida (Extremadura Central). PhD Thesis, Univ Salamanca, Salamanca, Spain pp 1-327

Gutiérrez-Alonso G, Fernández-Suárez J, Jeffries TE, Jenner GA, Tubrett MN, Cox R, Jackson SE (2003) Terrane accretion and dispersal in the northern Gondwana margin: an Early Paleozoic analogue of a long-lived active margin. Tectonophysics 365:221–232

Hoogewerff JA, van Bergen MJ, Vroon PZ, Hertogen J, Wordel R, Sneyers A, Nasution A, Varekamp JC, Moens HLE, Mouchel D (1997) U-series, Strontium-Neodynium-Lead isotope and trace element systematics across an active island arc-continent collision zone: implications for element transfer at the slab-wedge interface. Geochim Cosmochim Acta 61:1057–1072

Irvine TN, Baragar WRA (1971) A guide to chemical classification of common volcanic rocks. Can J Earth Sci 8:523–548

Irving AF, Frey FA (1978) Distribution of trace elements between garnet megacrysts and host volcanic liquids of kimberlitic to rhyolite composition. Geochim Cosmochim Acta 42:771–787

Julivert M, Fontboté JM, Ribeiro A, Conde L (1972) Mapa Tectónico de la Península Ibérica y Baleares a escala 1:1.000.000 y Memoria Explicativa. Publicaciones del Instituto Geológico y Minero de España, Madrid, pp1–113

Kohn MJ, Spear FS (1990) Two new barometers for garnet amphibolites with applications to eastern Vermont. Am Mineral 75:89–96

Krogh TE (1982) Improved accuracy of U-Pb zircon ages by the creation of more concordant systems using an air abrasion technique. Geochim Cosmochim Acta 46(4):637–649

Krogh Ravna E (1998) Distribution of Fe^{2+} and Mg between coexisting garnet and hornblende in synthetic and natural systems: an empirical calibration of the garnet-hornblende Fe-Mg geothermometer. Lithos 53:265–277

Krogh Ravna E (2000) The garnet-clinopyroxene Fe^{2+}-Mg geothermometer: an updated calibration. J Metamorph Geol 18: 211–219

Lancelot JR, Allegret A (1982) Radiochronologie U/Pb de l'orthogneiss alcalin de Pedroso (Alto Alentejo, Portugal) et évolution anté-hercynienne de l'Europe occidentale. Neues Jahrb Miner Abh 9:385–394

Lotze F (1945) Zur gliederung der varisziden der Iberischen Meseta. Geol Forsch 4:78–92

Ludwig KR (1993) Pbdat: a computer program for processing Pb–U–Th isotope data, version 1.24. Open-File Report 88–542, US Geological Survey, Reston, Virginia, pp 1–32

Ludwig KR (2001) User manual for Isoplot/Ex rev. 2.49. A geochronological toolkit for Microsoft Excel. Berkeley Geochronology Center, Berkeley, Spec. Publ. no. 1a, 56 pp
Martines Poyatps DJ (1997) Estrucura del Borde Meridional de la Zona Centroibérica y su relacción con el contacto entre las Zonas Centroibérica y de Ossa Morena. PhD Thesis, Univ. Granada, Granada, pp 1–255
McCulloch MT, Gamble AJ (1991) Geochemical and geodynamical constraints on subduction zone magmatism. Earth Planet Sci Lett 102(2–3):358–374
Miyashiro A (1978) Nature of alkalic volcanic rock series. Contrib Mineral Petrol 66:91–104
Murphy JB, Nance RD (1991) Supercontinent model for the contrasting character of Late Proterozoic Orogenic belts. Geology 19:469–472
Murphy JB, Eguíluz L, Zulauf G (2002) Cadomian Orogens, peri-Gondwanan correlatives and Laurentia–Baltica connections. Tectonophysics 352:1–9
Nance RD, Thompson MD (eds) (1996) Avalonian and related Peri-Gondwanan terranes of the circum-North Atlantic. Geol Soc Am Spec Pap 304:1–390
Nance RD, Murphy JB, Strachan RA, D'Lemos RS, Taylor GK (1991) Late Proterozoic tectono-stratigraphic evolution of the Avalonian and Cadomian terranes. Precambrian Res 53:41–78
Ochsner A (1993) U-Pb Geochronology of the Upper Proterozoic-Lower Paleozoic geodynamic evolution in the Ossa-Morena Zone (SW Iberia): constraints on the timing of the Cadomian Orogeny. PhD Thesis no. 10392, ETH, Zurich, Switzerland, pp 1–430
Ordóñez B (1998) Geochronological studies of the Pre-Mesozoic basement of the Iberian Massif: the Ossa Morena Zone and the Allochthonous Complexes within the Central Iberian Zone. PhD Thesis, no. 12940, ETH, Zürich, Switzerland, pp 1–235
Paquette JL, Pin C (2001) A new miniaturized extraction chromatography method for precise U-Pb zircon geochronology. Chem Geol 176:311–319
Paquette JL, Gleizes G, Leblanc D, Bouchez JL (1997) Le granite de Bassiés (Pyrénées): un pluton syntectonique d'âge Westphalien. Géochronologie U–Pb sur zircons. CR Acad Sci Paris 324:387–392
Pattison DRM (2003) Petrogenetic significance of orthopyroxene-free garnet + clinopyroxene + plagioclase ± quartz-bearing metabasites with respect to the amphibolite and granulite facies. J Metamorph Geol 21:21–34
Pearce JA (1982) Trace element characteristics of lavas from destructive plate related rocks. Wiley, London, pp 525–548
Peccerillo A, Taylor SR (1976) Geochemistry of Eocene calc-alkaline volcanic rocks from the Kastamonu area, northern Turkey. Contrib Mineral Petrol 58:63–81
Pereira MF (1999) Caracterizaçao da estructura dos dominios sententrionais da Zona de Ossa-Morena e seu limite com a Zona Centro-Ibérica, no nordeste Alentejano. PhD Thesis, Univ Évora, Évora, Portugal, pp 1–115
Pieren A (2000) Las sucesiones anteordovícicas de la región oriental de la Provincia de Badajoz y área contigua de la de Ciudad Real. PhD Thesis, Univ Complutense, Madrid, Spain, pp 1–379
Pin C, Joannon S (1997) Low-level analysis of lanthanides in eleven silicate rock reference materials by ICP-MS after group separation using cation-exchange chromatography. Geosci Newslett 21:43–50
Pin C, Santos Zalduegui JF (1997) Sequential separation of light rare-earth elements, thorium and uranium by miniaturized extraction chromatography : application to isotopic analyses of silicate rocks. Anal Chem Acta 339:79–89
Pin C, Liñán E, Pascual E, Donaire T, Valenzuela A (2002) Late Neoproterozoic crustal growth in the European Variscides: Nd isotope and geochemical evidence from the Sierra de Córdoba Andesites (Ossa-Morena Zone, southern Spain). Tectonophysics 352:133–151
Plank T, Langmuir CH (1998) The chemical composition of subducting sediment: implications for the crust and mantle. Chem Geol 145:325–394
Priem HNA, Boelrijk NAIM, Verschure RH, Hebeda EH, Verdurmen EAT (1970) Dating events of acid plutonism through the Paleozoic of the western Península. Eclogae Geol Helvet 63:255–274
Quesada C, Dallmeyer RD (1994) Tectonothermal evolution of the Badajoz-Córdoba shear zone (SW Iberia): characteristics and $^{40}Ar/^{39}Ar$ mineral age constraints. Tectonophysics 231:195–213
Ringuette L, Martignole J, Windley BF (1998) Pressure–temperature evolution of garnet-bearing rocks from the Jijal complex (western Himalayas, northern Pakistan): from high-pressure cooling to decompression and hydration of a magmatic arc. Geol Bull Univ Peshawar 31:167–168
Ringuette L, Martignole J, Windley BF (1999) Magmatic crystallization, isobaric cooling, and decompression of the garnet-bearing assemblages of the Jijal sequence (Kohistan Terrane, western Himalayas). Geology 27:139–142
Santamaría J (1995) Los yacimientos de fosfato sedimentario en el límite Precámbrico-Cámbrico del Anticlinal de Valdelacasa (Zona Centro-Ibérica). PhD Thesis, Univ Aut, Barcelona, 1–233 pp
Schäfer HJ (1990) Geochronological investigations in the Ossa-Morena Zone, SW Spain. PhD Thesis no. 9246, ETH, Zurich, Switzerland, pp 1–153
Scherer E, Münker C, Mezger K (2001) Calibration of the Lutetium-Hafnium clock. Science 293:683–687
Spear FS (1993) Metamorphic phase equilibria and pressure–temperature-time-paths. Mineral Soc Am, Washington, DC, pp 1–799
Stacey JS, Kramers JD (1975) Approximation of terrestrial lead isotope evolution by a two-stage model. Earth Planet Sci Lett 26:207–221
Sun SS, McDonough WF (1989) Chemical and isotopic systematics of oceanic basalts: implications for mantle composition and processes. In: Saunders AD, Norry MJ (eds) Magmatism in the ocean basins. Geoll Soc Spec Publ 42:313–345
Stampfli GM, von Raumer JF, Borel GD (2002) Paleozoic evolution of pre-Variscan terranes: from Gondwana to the Variscan collision. In: Martínbez Catalán JR, Hatcher RD, Arenas R, Díaz García F (eds) Variscan-Appalachian dynamics: the building of the Late Paleozoic basement. Boulder, Colorado, Geol Soc Am Spec Pap 364:263–268
Valladares MI, Barba P, Ugidos JM, Colmenero JR, Armenteros I (2000) Upper Proterozoic–Lower Cambrian sedimentary successions in the Central Iberian Zone (Spain): sequence stratigraphy, petrology and chemostratigraphy—implications for other European areas. Int J Earth Sci 89:2–20
Vidal G, Palacios T, Gámez-Vintaned JA, Díez Balda MA, Grant SWF (1994a) Neoproterozoic-early Cambrian geology and palaeontology of Iberia. Geol Mag 131:729–765
Vidal G, Jensen S, Palacios T (1994b) Neoproterozoic (Vendian) ichnofossils from Lower Alcudian strata in central Spain. Geol Mag 131:169–179
Vidal G, Palacios T, Moczydlowska M,Gubanov AP (1999) Age constraints from small shelly fossils on the early Cambrian terminal Cadomian Phase in Iberia. Geol Soc Stockholm 121:137–143
Von Raumer JF, Stampfli GM, Bussy F (2003) Gondwana-derived microcontinents: the constituents of the Variscan and Alpine collisional orogens. Tectonophysics 365:7–22
Vroon PZ, Van Bergen MJ, White WM, Varekamp JC (1993) Sr-Nd-Pb isotope systematics of Banda arc, Indonesia: combined subduction and assimilation of continental material. J Geophys Res 98:22349–22366
Wetherill GS (1956) Discordant uranium-lead ages, I. Trans Am Geophys Union 37:320–326
Wetherill GS (1963) Discordant uranium-lead ages, II. Discordant ages resulting from diffusion of lead and uranium. J Geophys Res 68:2957–2965

Wilson,M (1989) Igneous petrogenesis. Unwin Hyman, London, 466 pp

Yamamoto H, Nakamura E (1996) Sm-Nd dating of garnet granulites from the Kohistan complex, northern Pakistan. J Geol Soc Lond 153:965–969

Yamamoto H, Nakamura E (2000) Timing of magmatic and metamorphic events in the Jijal complex of the Kohistan arc deduced from Sm-Nd dating of mafic granulites. In: Khan MA, Treloar PJ, Searle MP, Jan MA (eds) Tectonics of the Nanga Parbat Syntaxis and the Western Himalaya. Geol Soc Lond Spec Publ 170:313–319

Zhou B, Hensen BJ (1995) Inherited Sm/Nd isotope components preserved in monazite inclusions within garnets in leucogneiss from East Antarctica and implications for closure temperature studies. Chem Geol 121:317–326